

Accurate Results from Perturbation Theory for Strongly Frustrated $S = \frac{1}{2}$ Heisenberg Spin Clusters

N.P. Konstantinidis and D. Coffey

Department of Physics, State University of New York at Buffalo, Amherst, NY 14260

(October 31, 2018)

We investigate the use of perturbation theory in finite sized frustrated spin systems by calculating the effect of quantum fluctuations on coherent states derived from the classical ground state. We first calculate the ground and first excited state wavefunctions as a function of applied field for a 12-site system and compare with the results of exact diagonalization. We then apply the technique to a 20-site system with the same three fold site coordination as the 12-site system. Frustration results in asymptotically convergent series for both systems which are summed with Padé approximants.

We find that at zero magnetic field the different connectivity of the two systems leads to a triplet first excited state in the 12-site system and a singlet first excited state in the 20-site system, while the ground state is a singlet for both. We also show how the analytic structure of the Padé approximants at $|\lambda| \simeq 1$ evolves in the complex λ plane at the values of the applied field where the ground state switches between spin sectors and how this is connected with the non-trivial dependence of the $\langle S^z \rangle$ number on the strength of quantum fluctuations. We discuss the origin of this difference in the energy spectra and in the analytic structures. We also characterize the ground and first excited states according to the values of the various spin correlation functions.

PACS numbers: 75.10.Jm Quantized Spin Models, 75.50.Ee Antiferromagnetics, 75.50.Xx Molecular Magnets

I. INTRODUCTION

The antiferromagnetic spin Heisenberg model has been the object of intense investigation through the years. Recently it has attracted enormous interest in the study of strongly correlated electron systems, which include the oxide superconductors [1] and low dimensional spin systems. In the limit where the on-site Coulomb repulsion is very strong, it is equivalent to the one band Hubbard model for half filling. The inclusion of competing interactions in it has led to novel quantum phases, making it appropriate for the study of quantum criticality [2].

The solution of the model was calculated by Bethe in one dimension for nearest neighbor interactions [3], but a solution in analytic form is lacking for two or three dimensions, except for special cases [4]. Approximation and numerical techniques that have been used include diagonalization of small clusters [5,6], Monte Carlo techniques [7], cluster expansions [8], spin wave expansions [9–11] and the density matrix renormalization group [12]. The methods that consider the full Hilbert space of the problem are limited by the size of the system, since the number of states is exponentially dependent on it. In Monte Carlo calculations the sign problem leads to loss of statistical accuracy, especially for frustrated systems [7].

An alternative approach to these techniques is the direct application of perturbation theory in which corrections to the classical treatment are calculated order by order in the strength of residual interactions, the effect of fluctuations left out in the mean field approximation. Although this approach can also be limited in the size of the systems which can be investigated due to the dimensionality of the Hilbert space, it is very different in that it provides analytic information on the effects of corrections to classical approximations and so complements the other approaches mentioned above. We use this approach to calculate the ground state wavefunction of two systems which have qualitatively different classical ground states, as we will explain below. We demonstrate that the differences survive in the exact spin $\frac{1}{2}$ ground states through the difference in the analytic structures of the Padé approximants derived from the perturbation expansions.

We consider the Heisenberg model on closed two dimensional spin $\frac{1}{2}$ systems which have three nearest neighbors. The antiferromagnetic interaction between the spins leads to frustration at the classical level. One such system is the 60 site cluster whose relative positions are the same as those of carbon atoms in C_{60} (from now on we will refer to n site systems with the spatial symmetry of the fullerenes as C_n). The 60 site system consists of 20 hexagons and 12 pentagons. Assuming a tight binding model for its electronic properties where there is one orbital per site and a strong Coulomb repulsion for double occupancy, the Heisenberg model on it gives an effective low energy description at half filling. This is a first approximation to the problem, since C_{60} is estimated to be in the intermediate and not in the strong coupling U regime [13]. The hopping matrix elements between sites on the same pentagon can be taken

to be different from the ones between sites on adjacent pentagons. This leads to two positive exchange constants J_1 and J_2 and the Hamiltonian is:

$$H = J_1 \sum_{\langle i,j \rangle}^{p.} \vec{S}_i \cdot \vec{S}_j + J_2 \sum_{\langle i,j \rangle}^{n.p.} \vec{S}_i \cdot \vec{S}_j . \quad (1)$$

J_1 refers to bonds between the same pentagon and J_2 to non-pentagon bonds, while $\langle \rangle$ stands for nearest neighbor interactions.

The classical ground state of the Heisenberg Hamiltonian has been determined on this and analogous C_n systems [13]. The magnetic properties of these ground states show an unexpected dependence on n . In some the magnetization is discontinuous in an applied field whereas in others it is the susceptibility which is discontinuous. It is of interest to determine whether this dependence is an artifact of the classical approximation or whether it is present in $S = \frac{1}{2}$ solutions. We use the classical C_n ground states to define an Ising Hamiltonian where the quantization axis at each site is determined by the direction of the spin vector in the classical ground state. Coherent states are defined along these axes and constitute a mean field approximation for the quantum ground state. In this way, each site has a local axis associated with it, in contrast to the basis where all spins are defined in the same coordinate system in spin space. From now on we call the former 'local basis', and the latter 'global basis'. The quantum fluctuations are then built around the classical directions. They are the terms added to the original mean field approximation, and they are multiplied with a parameter λ which varies from 0 to 1. When $\lambda = 1$, the full isotropic Heisenberg Hamiltonian is recovered. Thus the solution is generated as a series expansion in the perturbation parameter λ with application of perturbation theory, and the expansions of the ground state energy and wavefunction in the local axes basis are known. With this approach we can study the evolution of the system away from the classical ground state and towards the full quantum limit $\lambda = 1$.

However, the Hilbert space for the 60 site system is huge, consisting of $2^{60} = 1.15 \times 10^{18}$ states, so a perturbation treatment in the whole Hilbert space can only give a few orders. This is because the number of states involved in the calculation rapidly increases as the order and frustration increase [14]. In addition, since the spin axes are directed along the classical solution's directions, the total spin in the global basis is not a good quantum number of the Hamiltonian (when $\lambda < 1$), so a reduction of the number of states by focusing on a particular S^z value is not possible. Another way of gaining insight into the problem is to consider similar smaller systems, belonging to the same family. In all these systems there are $n_h = \frac{n}{2} - 10$ number of hexagons and 12 pentagons. The smallest member of the group is the 20 site system. Again, we consider $S = \frac{1}{2}$ spins sitting at their vertices.

The frustration of the Hamiltonians studied leaves its signature in the various series expansions generated by perturbation theory, producing functions with non-analytic structure in the complex λ plane. The presence of branch cuts limits absolute convergence within a circle centered at the origin with a radius of convergence smaller than 1 and the series are only asymptotically convergent in the full isotropic limit where $\lambda = 1$. Therefore, we employ analytic continuation with the use of Padé approximants. The structure of the functions in the λ plane depends strongly on the form of the perturbing Hamiltonian. We investigate the signature of the changes in the complex plane structure of the related functions as the perturbing Hamiltonian is varied. The generalization to complex variables has been proven useful in the study of phase transitions in the two dimensional Ising model in temperature T in a complex magnetic field [15]. The systems studied here are closed and do not possess a thermodynamic limit. However, knowledge of the structure in the complex coupling constant plane provides information about the functions studied [16]. It can also provide information for the evolution of instabilities. Here the only possible transitions are between $\langle S^z \rangle$ sectors with increasing magnetic field, where $\langle S^z \rangle$ is the expectation value of the z component of the spin in the global basis.

The classical ground state at zero magnetic field is doubly degenerate, since a flipping of all the spins does not change the energy. Consequently degenerate perturbation theory has to be applied [17]. This is done via a similarity transformation, and an effective 2×2 matrix is generated. This matrix provides information on the ground and first excited state, including the evolution of $\langle S^z \rangle$ as a magnetic field is varied. The structure of this matrix in the complex λ plane can be correlated with the transitions of the $\langle S^z \rangle$ number between different sectors as a function of the magnetic field.

The plan of this paper is as follows: in section II the method for the solution of the problem using perturbation theory is described. In section III this is applied to a twelve site system, C_{12} , where the results are compared with exact diagonalization and found to be in complete agreement. We also discuss how the analytic structure of perturbation theory is reflected in the magnetic properties. In section IV perturbation theory is applied to C_{20} and the results are tested by recovering expectation values for \vec{S}^2 and S^z very close to integer values. Here we contrast the magnetic field dependence of the analytic structure with the results found in the classical approximation. For both C_{12} and C_{20} ground and first excited state wavefunctions are calculated in applied magnetic fields and the dependence of their

magnetic properties on the strength of quantum fluctuations is determined. In the case of C_{20} , the ground and excited states at zero magnetic field are singlets. This result is in agreement with similar ones for strongly frustrated magnetic systems such as the Kagomé lattice and a one dimensional analogue of the pyrochlore lattice [18]. The non-magnetic nature of the excitation is attributed to the frustration and the connectivity of the system.

II. METHOD

The starting point in the calculation is the classical ground state. The Hilbert space is spanned by spin $\frac{1}{2}$ spinors determined by the classical solution. Local z_i axes are defined along the classical spin directions, and spin states are defined at each site such that the expectation value of the component of the spin along the axis equals its classical value:

$$\langle \begin{smallmatrix} \alpha_i \\ \beta_i \end{smallmatrix} | \vec{\sigma} | \begin{smallmatrix} \alpha_i \\ \beta_i \end{smallmatrix} \rangle = \vec{S}_i \quad , \quad (2)$$

where α_i, β_i are spinor coefficients and $|\vec{S}_i| = 1$. The coherent states [19] are products of spin states along these axes:

$$|\Psi_S\rangle = \prod_{i=1}^N |S_i\rangle = \prod_{i=1}^N \begin{smallmatrix} \alpha_i \\ \beta_i \end{smallmatrix} \quad , \quad (3)$$

where N is the number of spins in the system. Here we limit ourselves to these 2^N states out of the overcomplete basis of the coherent states. These are eigenstates of the unperturbed Hamiltonian H_0 and constitute an orthonormal basis. The classical ground states are the ones where all the spins are either 'up' or 'down' so that H_0 has the form of an Ising Hamiltonian with respect to the local quantization axes defined by the classical result. The fluctuations around the local z_i axes are raising and lowering spin operators, defined along the local x_i and y_i axes. These are included in the perturbing part H_1 which we scale with a parameter λ . Each x_i axis is defined in the azimuthal plane of the corresponding z_i axis and perpendicular to it, and then the y_i axis is constructed with the right hand rule. Due to the absence of a global z axis, the Hamiltonian takes a complicated form. The solution is generated in perturbation theory as a power series in λ . Therefore the Hamiltonian has the form:

$$H = H_0 + \lambda H_1 \quad , \quad (4)$$

where H_0 is the classical part and H_1 the quantum fluctuations.

There are two well known issues which complicate the application of perturbation theory. The first is the double degeneracy of the coherent states generated from the classical ground state in the absence of an applied magnetic field. This requires the use of degenerate perturbation theory. To overcome this problem, an effective Hamiltonian is constructed for the degenerate ground states, via a similarity transformation [17]. The Hamiltonian is transformed to a block diagonal form and its elements, as well as the coefficients of the Hilbert space states, which contribute to the perturbed wavefunctions, are expanded as power series in λ . Then recurrence relations can be written down for the effective Hamiltonian and the wavefunctions:

$$H_k^{eff}(m, \ell) = \langle m | H_1 | \Psi_{k-1}^{(\ell)} \rangle \quad , \quad (5)$$

$$\langle n | \Psi_k^{(\ell)} \rangle = \frac{1}{E_0 - E_n} (\langle n | H_1 | \Psi_{k-1}^{(\ell)} \rangle - \sum_{k'=1}^{k-1} \sum_{\ell'=1}^L H_{k-k'}^{eff}(\ell', \ell) \langle n | \Psi_{k'}^{(\ell')} \rangle) \quad . \quad (6)$$

Here k is the order of perturbation, $|m\rangle$ a degenerate ground state of H_0 , $|n\rangle$ a state in the Hilbert space different from $|m\rangle$, E_n its energy at the classical level and E_0 the classical ground state energy. L is the dimensionality of the degenerate subspace (here $L = 2$) and ℓ runs from 1 to L . The result of this calculation is an $L \times L$ (here 2×2) matrix whose eigenenergies are the ground state and the first excited state. This method can be applied for zero or non-zero magnetic field, where all the magnetic field terms in the Hamiltonian are included in the perturbation. If the magnetic field is included in H_0 non-degenerate perturbation theory can be applied in this case.

The second issue complicating the problem is that the perturbative part of the Hamiltonian generates series expansions whose radius of convergence does not extend to the isotropic limit $\lambda = 1$ but rather is limited to a circle with a radius smaller than 1. Therefore, we analytically continue outside the radius of convergence with the use of Padé approximants. These are described in detail in the literature [20]. The algorithms used for their calculation here are the determinant algorithm and the Viscovatov algorithm [21]. We now apply the method to two systems, C_{12} and C_{20} .

III. C_{12}

A smaller system with a geometry similar to the ones considered above is the truncated tetrahedron C_{12} [22], shown in figure 1. This is made up of four triangles and three hexagons, and looks like a closed triangular lattice. Every site is three fold coordinated, and bonds between sites on the same triangle (tr.) are called J_1 , while different triangle bonds (n.tr.) are named J_2 . The exact solution of the Heisenberg Hamiltonian has been found for this system and is used to check the results from perturbation theory here. At the classical level it was found to have a jump in the susceptibility at a critical value of an external magnetic field and so has similar properties to the systems discussed in reference [13]. As mentioned above the classical solution determines local axes of quantization z_i and determines H_0 . Spins belonging to the same triangle are coplanar at the classical level and each local x_i axis is defined in this plane. With application of the right hand rule the corresponding y_i axis is defined. With $\alpha = \frac{J_2}{J_1}$ the Hamiltonian becomes:

$$\frac{H}{J_1} = H_0 + \lambda H_1 \quad , \quad (7)$$

where

$$H_0 = \sum_{\langle i,j \rangle}^{tr.} \left(-\frac{1}{2}\right) S_i^z S_j^z + \alpha \sum_{\langle i,j \rangle}^{n.tr.} (-1) S_i^z S_j^z \quad , \quad (8)$$

$$\begin{aligned} H_1 = & \frac{1}{2} \sum_{\langle i,j \rangle}^{tr.} \left(\sin^2\left(\frac{\pi}{6}\right) S_i^+ S_j^- - \cos^2\left(\frac{\pi}{6}\right) S_i^+ S_j^+ - \cos\left(\frac{\pi}{6}\right) S_i^+ S_j^z + \cos\left(\frac{\pi}{6}\right) S_j^+ S_i^z \right) \\ & + \frac{\alpha}{2} \sum_{\langle i,j \rangle}^{n.tr.} e^{i\phi} S_i^+ S_j^+ + h.c. \quad , \quad (9) \end{aligned}$$

where $\phi = \tan^{-1}(2\sqrt{2})$. The coefficients reflect the dependence of the Hamiltonian on the classical spin directions. The Hamiltonian is complicated, since it includes any possible combination of raising, lowering and S_i^z operators, and has complex coefficients. There is no choice of the local coordinate systems that would make all the coefficients real, once the local z axes are fixed along the classical solution's directions. The local x_i and y_i can also be defined without reference to the specific form of the classical solution, as was stated in section II, but this results in a more complicated expression for the Hamiltonian.

A. Ground State Energy and Wavefunction

The ground state energy and the wavefunction coefficients are functions of λ and α . The $\alpha = 0$ case corresponds to four isolated triangles, while the $\alpha \rightarrow \infty$ case corresponds to spins forming singlets (dimers) via the J_2 bond. There is no further frustration when assembling the tetrahedron from the individual triangles, since this costs nothing in energy for the classical spins. Consequently for this system the classical ground state is independent of α and the quantum fluctuations select a unique ground state when $\lambda \neq 0$. This is reminiscent of the order-disorder transition induced by quantum fluctuations for frustrated systems [23]. The effective Hamiltonian for the two degenerate ground states has the following form:

$$H^{eff} = \begin{pmatrix} A_N(\lambda) & B_N(\lambda) \\ C_N(\lambda) & D_N(\lambda) \end{pmatrix} \quad , \quad (10)$$

where $A_N(\lambda)$, $B_N(\lambda)$, $C_N(\lambda)$ and $D_N(\lambda)$ are polynomials in λ of Nth order, the order of perturbation. λ can assume complex values, since we are also interested in the structure of the functions in the complex plane. The coefficients of series $C_N(\lambda)$ and $D_N(\lambda)$ are complex conjugates of the coefficients of $B_N(\lambda)$ and $A_N(\lambda)$ respectively. Therefore, in the case of physical interest where λ is real, $C_N(\lambda)$ and $D_N(\lambda)$ are the complex conjugates of $B_N(\lambda)$ and $A_N(\lambda)$ respectively. Diagonalization of the matrix in the latter case shows that its eigenvalues are real, as expected. The two classical ground states, $|0\rangle$ and $|\tilde{0}\rangle$, evolve in the following manner as functions of λ :

$$|\Psi_0\rangle_N = |0\rangle + \sum_{n=1}^N \lambda^n |\Psi_n\rangle = |0\rangle + \sum_{i=1}^{d-L} F_N^i(\lambda) |i\rangle \quad , \quad (11)$$

and similarly for $|\Psi_{\tilde{0}}\rangle_N$, where $F_N^i(\lambda)$ are polynomials of N th order in λ with complex coefficients, $|i\rangle$ is a Hilbert space vector different from $|0\rangle$ and $|\tilde{0}\rangle$ and d is the dimensionality of the Hilbert space. L is again the dimensionality of the degenerate subspace (here $L = 2$).

1. Analytic Continuation

The next step is to analytically continue the polynomials $A_N(\lambda)$, $B_N(\lambda)$, $C_N(\lambda)$, $D_N(\lambda)$ and $F_N^i(\lambda)$. Then the 2×2 matrix is diagonalized and the energies as well as the wavefunctions are known. This gives the ground and the first excited state at each value of λ . For C_{12} the dimensionality of the Hilbert space is $d = 2^{12} = 4096$.

The ground state energy for different α 's is given by the converged value of $E_N^g(\lambda)$, which is the lowest eigenvalue for the N th order approximant. The criterion for convergence is that at order N mean square fluctuations should be 1% of the mean value for the 7 approximants placed around the N th order (i.e., $N - 3, \dots, N, \dots, N + 3$). This is easily satisfied for small values of N when $\lambda < 0.5$ for $\alpha = 1$, but the mean square fluctuations increase for larger values of α . The dependence on N for different values of α can be understood by looking at the structure of $A_N(\lambda)$ in the complex coupling constant plane (figures 2 and 3) which is discussed below. The analytically continued form for the polynomials is given as the ratio of two polynomials defined in the complex λ plane so that, for example:

$$A_N(\lambda) \rightarrow A_N^{a.c.}(\lambda) = \frac{P_N(\lambda)}{Q_N(\lambda)}, \quad (12)$$

where *a.c.* stands for analytically continued. For λ on the real axis $D_N^{a.c.} = (A_N^{a.c.})^*$ and $C_N^{a.c.} = (B_N^{a.c.})^*$ guaranteeing real eigenvalues for real λ . The structure is revealed by looking at zeros and poles of $A_N^{a.c.}(\lambda)$ for complex λ . These are the roots of $P_N(\lambda)$ and $Q_N(\lambda)$. Frustration leads to branch cuts in the λ plane which are given by lines of mixed zeros and poles of $A_N^{a.c.}(\lambda)$. This is how the single valued $A_N^{a.c.}(\lambda)$ tries to reproduce a multi-valued function associated with a cut in the complex plane. This structure is shown for $\alpha = 1$ in figure 2 and for $\alpha = 2$ in figure 3, for $N = 220$. The radius of convergence λ_c (circles) shrinks as α increases and for $\lambda > \lambda_c$ the perturbation expansion is asymptotically convergent. This indicates that more orders are needed for Padé approximants to converge as the ratio $\frac{\lambda}{\lambda_c}$ increases. One explanation for this is that, as α increases, the classical ground state is not as good starting point as for small λ , since the spins tend to form singlets via the J_2 bond in the quantum limit. Thus it gets harder to reach the quantum state from the ordered classical ground state, the former made up of independent singlets on the non-triangle bonds at the limit $\frac{J_2}{J_1} \rightarrow \infty$.

2. Numerical Precision

As we go to higher orders in perturbation theory the number of calculations goes up, increasing the possibility for significant propagation of numerical error [24]. To extend the calculation to higher orders, the package MPFUN was used [25], which allows arithmetic to very high precision, limited only by machine specifications. The perturbation and analytic continuation were done by using typically 94 digits precision in MPFUN, except in some cases where 194 digits were used.

To reduce memory requirements and execution time, perturbation theory was first run in double precision. After the states with equal coefficients or coefficients differing only in sign (in real and/or imaginary part) due to symmetry were identified, the program was run with MPFUN, taking advantage of these symmetries. Thus the scale of the calculation was significantly reduced. The time required to get 250 orders in perturbation theory was approximately thirty five minutes, when eight processors were used in parallel on a SGI machine. These were IP27 processors with a frequency of 250 MHz. We typically used 250 orders to get convergence for fields smaller than J_1 .

A second criterion of convergence comes from the total spin component $\langle S^z \rangle$, which is a good quantum number for the Hamiltonian in the isotropic case where $\lambda = 1$. If the analytically continued wavefunction coefficients converge, then the calculation of $\langle S^z \rangle$ should yield an integer in an applied field. Any deviation from an integer value indicates lack of convergence, which could be due to insufficient orders of perturbation theory used or propagation of numerical error, and indicates that higher numerical accuracy is needed. This criterion is more stringent since now all the coefficients $F_N^i(\lambda)$ have to converge but once convergence is achieved any expectation value can be calculated, since the knowledge of the wavefunction fully solves the problem. Since all the states in the Hilbert space determined by the local z axes contribute to the ground and first excited state coefficient functions, the calculated wavefunction is essentially exact.

3. Degeneracy

In the absence of an applied field states with different $\langle S^z \rangle$ values are degenerate and the excited state, a triplet in C_{12} , is a linear combination of $S^z = 0, \pm 1$ states. However it is found that starting in the $S^z = 0$ sector as we do the perturbed state stays in this sector for all λ for both ground and excited state at $h=0$. Although this degeneracy is lifted by the applied field, there is an additional degeneracy due to the geometrical symmetries of C_{12} . The exact diagonalization shows that there are three degenerate triplet states at the first excitation energy so that even in an applied field the excited state with $S^z = 1$ is triply degenerate. Choosing a particular classical ground state to generate the starting states $|0\rangle$ and $|\bar{0}\rangle$ picks out a linear combination of these degenerate states.

4. Correlation Functions

After the calculation of the ground state wavefunction, its correlation functions can be directly evaluated. In C_{12} there are five kinds of qualitatively different correlation functions, two of which refer to nearest neighbors. In figures 4 and 5 these are plotted as a function of the strength of the quantum fluctuations λ for the case $\alpha = 1$ for the ground and excited states respectively. The magnitude of the correlation function $\langle \vec{S}_1 \cdot \vec{S}_9 \rangle$ is smaller than 0.02 and is not plotted. For $\lambda = 1$ the solution of the full isotropic case agrees with the one found from exact diagonalization [22]. The nearest neighbor correlation functions are $\langle \vec{S}_1 \cdot \vec{S}_2 \rangle = -0.125$ and $\langle \vec{S}_1 \cdot \vec{S}_4 \rangle = -0.250$ at the classical level where $\lambda = 0$. Spins 1 and 4 are antiparallel, while $\langle \vec{S}_1 \cdot \vec{S}_2 \rangle$ is one half of $\langle \vec{S}_1 \cdot \vec{S}_4 \rangle$.

In the ground state (figure 4) $\langle \vec{S}_1 \cdot \vec{S}_2 \rangle$ increases in magnitude with λ and at $\lambda = 1$ equals -0.183 , being roughly 50% bigger than its classical value. $\langle \vec{S}_1 \cdot \vec{S}_4 \rangle$ increases in magnitude as the quantum fluctuations become stronger and reaches its maximum just before $\lambda = 0.8$. Then it doesn't change significantly and its magnitude at $\lambda = 1$ is more than two times larger than its classical one, being equal to -0.586 . This is because as the perturbation is turned on adjacent spins belonging to different triangles want to create singlet bonds due to their J_2 interaction. The value of $\langle \vec{S}_1 \cdot \vec{S}_4 \rangle$ at $\lambda = 1$ is close to the value for a singlet state between two spins, which is -0.750 . The other two correlation functions have a non-trivial dependence on λ , but their values in the isotropic case do not significantly differ from their classical ones.

The excited state correlation functions of figure 5 do not differ significantly from the ones of figure 4. However, we observe a smaller value for $\langle \vec{S}_1 \cdot \vec{S}_5 \rangle$ compared with the ground state value, while $\langle \vec{S}_1 \cdot \vec{S}_4 \rangle$ has a smaller magnitude at $\lambda = 1$ again compared to the ground state value indicating a more triplet character for this bond.

In figures 6 and 7 we plot the correlation functions for $\alpha = 2$. We observe that for both the ground and the excited state all the correlations decrease in magnitude, except the ones between neighboring spins connected via the J_2 bond. The value of $\langle \vec{S}_1 \cdot \vec{S}_4 \rangle$ in the ground state is now -0.697 , approaching the singlet value -0.750 even closer.

B. Magnetic Field

We next introduce a magnetic field in the problem and study the ground and excited states as a function of λ . There are two possible approaches to this calculation. The first is to perturb around the zero magnetic field classical ground state. The second is to calculate the classical ground state in the presence of a magnetic field, and then apply perturbation theory. Because the field breaks the time reversal symmetry, the classical ground state is non-degenerate, and in the second case non-degenerate perturbation theory is used. The results of the two methods should agree at the isotropic limit, $\lambda = 1$. However, their dependence on λ is different.

1. Degenerate case. Field independent classical ground state.

The Hamiltonian for the first method has the form:

$$\frac{H}{J_1} = H_0 + \lambda(H_1 + H_2) , \quad (13)$$

where H_0 and H_1 were defined before and H_2 is the part that relates to the magnetic field. Specifically:

$$H_2 = -h \sum_{i=1}^N \cos\theta_i S_i^z + \frac{h}{2} \sum_{i=1}^N \sin\theta_i (S_i^+ + S_i^-) . \quad (14)$$

h is the strength of the magnetic field in units of J_1 and θ_i the classical solution's angles with the global z axis. The direction of the magnetic field is taken along the global z axis, so it is perpendicular to the plane of one of the four triangles of the system. The spins belonging to any triangle are coplanar in the classical case (in spin space), and they can be chosen to lie in the physical plane of the triangle.

2. $\langle S^z \rangle$

For $\lambda = 1$, the ground state lies in the $S^z = 0$ sector when there is no magnetic field. $\langle S^z \rangle$ is defined along the global z axis, and it commutes with the Hamiltonian (13) at $\lambda = 1$. As the field is turned on the energy of the ground state, which is a singlet, won't change at the isotropic limit. However, the triplet excited state has $S^z = 1$ there, and its energy decreases linearly with the magnetic field due to the Zeeman term. At a critical value of the field the triplet state energy becomes equal to the one of the singlet state, so the triplet state becomes the ground state. As the magnetic field increases further the ground state moves towards spin sectors with higher value of S^z , until the magnetization saturates. The results for the energies found from perturbation theory and analytic continuation are found in figure 8, and they reproduce the exact values ($\lambda = 1$). By extrapolation of the straight lines which give the ground and the first excited energy back to zero field, we recover the energies of excited states in the zero field case. The diagonalization of the effective Hamiltonian matrix gives the following eigenenergies:

$$E_{1,2} = \frac{A_N^{a.c.}(\lambda) + D_N^{a.c.}(\lambda)}{2} \mp \left| \sqrt{B_N^{a.c.}(\lambda)C_N^{a.c.}(\lambda) + \left(\frac{A_N^{a.c.}(\lambda) - D_N^{a.c.}(\lambda)}{2}\right)^2} \right|, \quad (15)$$

where $A_N^{a.c.}(\lambda)$, $B_N^{a.c.}(\lambda)$, $C_N^{a.c.}(\lambda)$ and $D_N^{a.c.}(\lambda)$ are the analytically continued values of the corresponding polynomials of N th order. At the critical fields at which the two states exchange 'roles' as the ground and the first excited state, the square root goes to zero at $\lambda = 1$. This occurs when $B_N^{a.c.}$ and the imaginary part of $A_N^{a.c.}$ go to zero. In this way, we start from two degenerate ground states and we end up with two degenerate states.

The strict criterion for successful convergence of the wavefunctions is the calculation of the $\langle S^z \rangle$ number. This should be an integer at $\lambda = 1$. We calculate its evolution with λ in the global spin basis, where the quantization axis is the same for all spins. The expression for its expectation value $\langle S^z \rangle$ is:

$$\langle S^z \rangle = \frac{\langle \Psi_0 | S^z | \Psi_0 \rangle + |G|^2 \langle \Psi_{\bar{0}} | S^z | \Psi_{\bar{0}} \rangle + 2Re(G \langle \Psi_0 | S^z | \Psi_{\bar{0}} \rangle)}{\langle \Psi_0 | \Psi_0 \rangle + |G|^2 \langle \Psi_{\bar{0}} | \Psi_{\bar{0}} \rangle + 2Re(G \langle \Psi_0 | \Psi_{\bar{0}} \rangle)}, \quad (16)$$

where G is given by

$$G = \frac{\frac{A_N^{a.c.}(\lambda) - D_N^{a.c.}(\lambda)}{2} \pm \sqrt{B_N^{a.c.}(\lambda)C_N^{a.c.}(\lambda) + \left(\frac{A_N^{a.c.}(\lambda) - D_N^{a.c.}(\lambda)}{2}\right)^2}}{B_N^{a.c.}(\lambda)}. \quad (17)$$

The plus sign corresponds to the ground state and the minus sign to the excited one. The magnitude of this coefficient is 1 for any real λ , since in this case $D_N^{a.c.} = (A_N^{a.c.})^*$ and $C_N^{a.c.} = (B_N^{a.c.})^*$. The accurate calculation of the wavefunctions at the critical fields h_c involves taking the limit $\lim_{\lambda \rightarrow 1} G(\lambda)$. In this case the magnitude of $B_N^{a.c.}(\lambda)$ as well as the imaginary part of $A_N^{a.c.}(\lambda)$ go to zero, thus both the numerator and denominator vanish. The success of the analytic continuation is such that the calculation of $A_N^{a.c.}(\lambda)$ and $B_N^{a.c.}(\lambda)$ is so accurate after analytic continuation that the result $\lim_{\lambda \rightarrow 1} G(\lambda) = \pm 1$ is recovered and this is reflected in the calculated $\langle S^z \rangle$. The calculation was done for various fields for $\alpha = 1$, and the results are shown in figures 9 and 10. There it is shown that indeed $\langle S^z \rangle$ assumes integer values when $\lambda = 1$, confirming the success of analytic continuation. For example, when $h = 0.7$, at $\lambda = 1$ $\langle S^z \rangle = 0.99999999998$ for the ground state and $\langle S^z \rangle = 1.0 \times 10^{-11}$ for the excited state.

As seen in figure 9, the quantum fluctuations raise the value of $\langle S^z \rangle$ for small values of the magnetic field, but eventually it goes to zero at the isotropic limit. However, just above the transition to the $S^z = 1$ sector, which occurs at $h_{c1} = 0.6878$ in agreement with the exact answer, $\langle S^z \rangle$ has a non-trivial behavior for intermediate λ 's before assuming the value equal to 1. Thus for $h = 0.688$ there is a rapid change in the magnetization at a value of λ close to 1. There is competition between the 0 and 1 spin sector for the ground state, and finally the quantum fluctuations lead to the latter. The magnetic field terms of the perturbing Hamiltonian favor a magnetized ground state, while the rest favor zero spin. The sudden change in $\langle S^z \rangle$ as a function of λ moves closer to $\lambda = 1$ as $h \rightarrow h_c$ from below. If we go further away from this critical field, the jump is pushed towards smaller values of λ , and eventually it vanishes. Similar effects are observed in figure 10, which includes the corresponding graphs for the excited state. In this case, the excited state has $S^z = 1$ below and $S^z = 0$ above the transition. The conclusion is that there is a 'window' around the critical field where the λ dependence of $\langle S^z \rangle$ is very strong.

As the magnetic field gets bigger, more terms are needed to analytically continue the wavefunction so that the spin number assumes the proper integer values. There is also a need for greater numerical precision, due to the increased number of calculations which tend to propagate the numerical errors [24], and so 194 digits of MPFUN accuracy were used. The transition between the $S^z = 1$ and $S^z = 2$ spin sectors for the ground state takes place at $h_{c2} = 0.9869$. For a magnetic field equal to 1.01, 501 orders were generated to get convergence. This requirement for more orders in perturbation theory and more accuracy makes the calculation of the factor G of equation (16) harder as the second critical field is approached. The behavior of $\langle S^z \rangle$ as a function of λ is shown in figure 11, where the $\langle S^z \rangle$ value of the ground state remains constant over a range of λ , and eventually “jumps” to the final value $\langle S^z \rangle = 2$. On the other hand, the excited state $\langle S^z \rangle$ approaches 2 close to $\lambda \approx 1$ only to settle at 1 when $\lambda = 1$.

Non-monotonic behavior of the quantum number S^z near a transition is observed for other values of J_2 as well. These are shown in figures 12 and 13, for J_2 values equal to 0.8 and 1.8. For the second case the higher value of J_2 stabilizes the spin value for λ 's close to 1. It was observed that convergence was harder to get as J_2 and/or h were increased, for the reasons already mentioned.

3. Correlation Functions

Although the calculated eigenstates at $\lambda = 1$ are independent of magnetic field they do depend on the field for intermediate values of λ . This can be seen clearly in $\langle S^z \rangle$ as a function of λ in figures 9 and 10. As pointed out previously the choice of the starting classical ground state picks out a particular linear combination of the three degenerate ($S = 1, S^z = 1$) states. Different linear combinations lead to different values of the $\langle \vec{S}_i \cdot \vec{S}_j \rangle$. However when adding the values of nearest neighbor $\langle \vec{S}_i \cdot \vec{S}_j \rangle$ for different choices of starting classical ground states the values of the energies, calculated directly in equation (15), are recovered.

A further check on the two point correlation functions calculated for the wavefunctions is $\langle \vec{S}^2 \rangle = \sum_{i,j} \langle \vec{S}_i \cdot \vec{S}_j \rangle$. Calculating $\langle \vec{S}^2 \rangle$ in the ground and excited state at $h = 0.7$ we find 2.00188 and -0.0028361 consistent with $\langle S^2 \rangle = S(S+1)$ for $S = 1$ and $S = 0$. This measurement tests the accuracy of all two point correlation functions. The ones for nearest neighbors for $h = 0.7$ are plotted in figures 14 and 15 for the ground and excited states. Comparing these with the λ dependence of the states in figures 6 and 7, the only difference is a non-monotonic dependence at $\lambda \simeq 0.5$ especially for the nearest neighbor correlation functions $\langle \vec{S}_1 \cdot \vec{S}_2 \rangle$ and $\langle \vec{S}_1 \cdot \vec{S}_4 \rangle$.

4. Analytic Structure

The motion of the zero of the square root appearing in equations (15) and (17) in the complex λ plane can be traced out with the help of the Padé approximants, which are ratios of two polynomials. Since the analytic continuation was quite successful in the vicinity of $\lambda = 1$, we can look for the structure of approximants in this area. To this end, we consider the function

$$B_N^{a.c.}(\lambda)C_N^{a.c.}(\lambda) + \left(\frac{A_N^{a.c.}(\lambda) - D_N^{a.c.}(\lambda)}{2} \right)^2, \quad (18)$$

which is inside the square root in equations (15) and (17), and we plot the zeros of the numerator and the denominator of the approximants as a function of the magnetic field. The approximants were generated with 220 orders of perturbation theory (the order of the numerator and the denominator of the Padé approximant is one half of this number). In figure 16 the complex plane structure is plotted for a magnetic field $h=0.688$. The Padé approximant is seen to reproduce the branch cuts of the function in the complex plane. There are also zeros and poles in the complex plane not falling on any of the branch cuts. These are present only in approximants of specific order and they are artifacts of the analytic continuation. It can be seen how the zeros of equation (18) appear in the complex λ plane close to $\lambda = 1$. The coefficients of the expansion of (18) are real, so the zeros and the poles appear in complex conjugate pairs.

Another feature of the picture is that it is asymmetric with respect to the imaginary λ axis. This asymmetry gets more and more pronounced with increasing field. This is because negative λ 's correspond to different ferromagnetic couplings between neighboring sites, and these interactions favor aligned spins, a state similar to the one favored by the magnetic field. In this case it is more difficult to get convergence because of the competition of the classical antiferromagnetic interactions with the quantum ferromagnetic ones and the magnetic field. Consequently the radius of convergence is smaller.

In figure 17 the roots of the approximants are plotted for various magnetic fields close to $h_{c1} = 0.6878$ in the vicinity of $\lambda = 1$. The zeros of the square root approach $\lambda = 1$ in conjugate pairs and they finally hit the axis at the transition. As the strength of the field is further increased, the roots move away from $\lambda = 1$ in the opposite direction. We see this behavior in a small range of the fields around the transition with roots around $\lambda = 1$, which is reflected in the rapid non-monotonic variation of $\langle S^z \rangle$ around the critical field. Since the square root of function (18) has to eventually be taken, its zeros will turn into branch points in the complex λ plane.

5. Non-degenerate case. Field dependent classical ground state.

The alternative approach to the problem is to calculate the classical ground state in the presence of the magnetic field, and then introduce the remaining terms as perturbation. In this case the Hamiltonian is:

$$\frac{H}{J_1} = H_0 + H'_0 + \lambda(H_1 + H'_2) , \quad (19)$$

where:

$$H'_0 = -h \sum_{i=1}^N \cos\theta_i S_i^z , \quad (20)$$

$$H'_2 = \frac{h}{2} \sum_{i=1}^N \sin\theta_i (S_i^+ + S_i^-) . \quad (21)$$

and H_0 and H_1 have already been defined in equations (8) and (9). Since the magnetic field breaks the degeneracy of the classical ground state Rayleigh-Schrödinger perturbation theory can be applied directly for the wavefunctions. The results after the analytic continuation are shown in figure 18. This method can be compared with the one of the previous section only at $\lambda = 1$, where in both cases the isotropic Heisenberg Hamiltonian is recovered. Starting from the field dependent classical ground state is not any better as far as computer memory and execution time is concerned, since symmetries reduce memory requirements at the same level in both cases. However, the first method also gives the ground and first excited state very accurately, consequently the approach of the transitions between S^z sectors as a function of the applied magnetic field is easily seen. On the other hand, the second method works better for higher fields, since now the classical ground state is related to the strength of the magnetic field, thus it has a non-zero value for $\langle S^z \rangle$. Various fields up to $h = 1.3$ were employed in the calculation. The results for the energy agree with the exact diagonalization answer [22].

Looking at figure 18, we see the dependence of $\langle S^z \rangle$ on λ is not monotonic for the various magnetic fields. This can be attributed to the fact that the starting point is now the magnetic field dependent classical ground state. The terms in the Hamiltonian related to the magnetic field tend to increase the spin, while the rest favor a zero spin quantum state, thus there is competition between the two at the classical and quantum level. In the degenerate case the field dependent terms entered only in the perturbing part of the Hamiltonian, making the perturbation stronger and dominant in the determination of S^z for higher λ 's.

The structure of the analytic continuation of the energy was also studied in the non-degenerate case, and it was consistent with the structure found from the degenerate perturbation. For a magnetic field $h = 0.8$ the expression in equation (17) has a zero at $\lambda_1 \approx 0.788 + 0.337i$, while the analytically continued function for the energy in the non-degenerate case has a branch cut which starts at a value of λ equal to $\lambda_2 \approx 0.898 + 0.217i$ and extends almost parallel to the x axis. Since $\sqrt{|\lambda_1|} \simeq |\lambda_2|$, the branch cut of the square root in the degenerate case corresponds to the one of the non-degenerate case demonstrating the consistency of the two approaches starting from the classical ground state in the absence of a magnetic field and the magnetic field dependent classical ground state.

IV. C_{20}

Next we consider the 20 site system on the vertices of a dodecahedron, shown in figure 19. In C_{20} there is only one kind of bond, which we call J, and each atom has three nearest neighbors as in the C_{12} case. In the classical solution spins belonging to the same pentagon are not coplanar [13], and the energy per bond is $-\frac{\sqrt{5}}{3} = -0.7454$. This is bigger than the energy per bond for the coplanar spins on an isolated pentagon, which is $\cos(\frac{4\pi}{5}) = -0.8090$. Thus when

the dodecahedron is assembled from the individual pentagons there is a cost in energy, in contrast to the twelve-site system case. This system has a discontinuity in $\langle S^z \rangle$ as a function of the magnetic field at the classical level unlike the twelve-site system. The discontinuity has a magnitude of 0.64 and occurs at a magnetic field $h = 1.432J$. This is also the case for C_{60} whereas in C_{12} , C_{70} and C_{84} there is a discontinuity in the slope of the magnetization with applied field [13]. We start again from the classical ground states and perturb them with the quantum fluctuations. The difference now is that the exact solution of the problem is not known and the Hilbert space is much larger with $2^{20} = 1,048,576$ states.

The question we wish to address is whether the differences between C_{12} and C_{20} seen at the classical level in magnetic properties survive for the $S = \frac{1}{2}$ case. As we will show below these differences do survive and are seen in the analytic structure of the perturbation theory for the two systems. Since spins are not coplanar at the classical level, the Hamiltonian, which is defined as described in section II, assumes the following complicated form:

$$\frac{H}{J} = H_0 + \lambda H_1, \quad (22)$$

$$H_0 = -\frac{\sqrt{5}}{3} \sum_{\langle i,j \rangle} S_i^z S_j^z, \quad (23)$$

$$H_1 = \sum_{\langle i,j \rangle} (\alpha_{ij} S_i^+ S_j^+ + \beta_{ij} S_i^+ S_j^- + \gamma_{ij} S_i^+ S_j^z + \delta_{ij} S_j^+ S_i^z) + h.c., \quad (24)$$

where α_{ij} , β_{ij} , γ_{ij} and δ_{ij} are complex coefficients defined analytically. For example, for the $\vec{S}_1 \cdot \vec{S}_2$ term $\alpha_{12} = \frac{1}{4}(1 + \frac{\sqrt{5}}{3})$, $\beta_{12} = \frac{1}{8}(1 - \frac{\sqrt{5}}{3})(1 - \sqrt{3}i)$, $\gamma_{12} = -\frac{1}{6}(1 + \sqrt{3}i)$ and $\delta_{12} = \gamma_{12}^*$. Since here the starting point is the classical ground state, defining a local z axis at each site, the coefficients of H_1 are in general different for different bonds. Furthermore they are complex because of the non-planar character of the spins in the classical ground state. We apply the same methods towards the solution as in the twelve-site system case. The elements of the 2×2 effective Hamiltonian matrix H^{eff} in equation (10) are now real for all applied magnetic fields.

A. Ground and Excited States

The energies and wavefunctions of the two lowest lying states were calculated up to $h = 0.72J$. The ground state (\circ) and the excited state (\diamond) are shown in figure 20. By drawing straight lines through the energies and extrapolating to zero field the lowest energy state in each spin sector is recovered, as well as the second lowest energy in the $S = 0$ sector. We find these energies to be $E_1(S = 0) = -9.722J$, $E_2(S = 0) = -9.345J$, $E_3(S = 1) = -9.208J$ and $E_4(S = 2) = -8.523J$. The magnetic field dependence is given by a Zeeman term $-h \sum_{i=1}^{20} S_i^z$. Unlike C_{12} the first excited state at $h \leq 0.137$ is a singlet rather than a triplet [18].

B. Correlation Functions

In figure 21 we plot the lambda dependence of the expectation value $\langle S^z \rangle$ for $h = 0.4$. We see a behavior similar to the one of C_{12} , as the ground state assumes the value -2.7×10^{-8} and the excited state the value 0.9999997 at $\lambda = 1$. Again this points to the accuracy of the calculated wavefunctions. The ferromagnetic or antiferromagnetic character of the correlation between any two sites remains the same in the ground state and the two lowest lying excited states at $h = 0$. In each of these states the nearest neighbor correlation ~ -0.3 , while all other $\langle \vec{S}_i \cdot \vec{S}_j \rangle$ have magnitudes $\sim 0.03 \rightarrow 0.08$ at $\lambda = 1$. Correlation functions are plotted for the lowest lying singlet and triplet states at $h = 0.4$, where they are the ground and first excited state in figures 22 and 23. We first consider the nearest neighbor correlations. For the singlet state, figure 22, the $\langle \vec{S}_1 \cdot \vec{S}_2 \rangle$ and $\langle \vec{S}_1 \cdot \vec{S}_6 \rangle$ are equal only at $\lambda = 0$ and $\lambda = 1$. The λ dependence for $0 < \lambda < 1$ depends on both the starting classical ground state and the value of h . For the lowest energy singlet state, $\langle \vec{S}_1 \cdot \vec{S}_2 \rangle$ and $\langle \vec{S}_1 \cdot \vec{S}_6 \rangle$ grow in magnitude from their classical value, -0.186 at $\lambda = 0$, to -0.324 at $\lambda = 1$ for all nearest neighbor correlations. Thus they are comparable to the value of the nearest neighbor correlation in the ground state of an isolated pentagon, -0.375 .

In the lowest lying $S = 1$ $S^z = 1$ state, figure 23, two values of the nearest neighbor correlation functions are present, -0.297 and -0.327 at $\lambda = 1$. This state can be described by considering the bonds on a pentagon, on its

diametrically opposite mirror and on a chain formed by the 10 remaining sites. On these bonds $\langle \vec{S}_i \cdot \vec{S}_j \rangle = -0.297$ while on the bonds connecting the chain to the two pentagons $\langle \vec{S}_i \cdot \vec{S}_j \rangle = -0.327$. Since this configuration can be chosen in six different ways the triplet $S = 1$ $S^z = 1$ state is six fold degenerate. There is little difference between the next nearest neighbors and more distant correlations in the singlet and triplet states. The quantum fluctuations significantly reduce the magnitude of these correlations compared with their classical values at $\lambda = 0$.

As a further check of the accuracy of the wavefunction the calculated values of these correlations give for $\langle \vec{S}^2 \rangle = \sum_{i,j} \langle \vec{S}_i \cdot \vec{S}_j \rangle$ the value -0.00089 for the ground state and the value 1.99154 for the excited state at $\lambda = 1$. These are consistent with the calculated $\langle S^z \rangle$ values in figure 21. The change in the value of $\langle \vec{S}^2 \rangle$ between the singlet and triplet states comes from changes in all the $\langle \vec{S}_i \cdot \vec{S}_j \rangle$. The change due to the nearest neighbor $\langle \vec{S}_i \cdot \vec{S}_j \rangle$'s is ~ 1 and the rest comes from small changes, ~ 0.005 , from the other bonds. This suggests that there is no simple characterization of the excited states.

In the classical ground state all the spins in the top and bottom pentagons have the same azimuthal angle α with the z axis, which is later taken to be the direction of the magnetic field. The rest of the spins form a different angle β with the z axis, so there are two different angles in the classical solution. There are only two distinct functions $\langle \vec{S}_i \cdot \vec{h} \rangle$ of the spins for the calculated states in the magnetic field, and they represent these two kinds of sites in the classical ground state. They were calculated for $i = 1$ and 6 and they are plotted in figure 24 for the ground and the excited state. They are consistent with $\langle \sum_i \vec{S}_i \cdot \vec{h} \rangle = \langle S^z \rangle h$ calculated in the ground and excited state in figure 21.

For $h \leq 0.137$ the excited state is a singlet. This state has the same symmetry as in the triplet state with two types of nearest neighbor bonds equal to -0.304 and -0.324 . As in the triplet case the longer range correlations, both ferromagnetic and antiferromagnetic are still comparable in magnitude and ~ 0.05 .

C. Analytic Structure

Next we study the structure of the analytic continuation of the off-diagonal element $B_N^{a.c.}(\lambda)$. In figure 25 we plot the structure at a magnetic field equal to 0.3 . Again we observe the asymmetry with respect to the y axis. As in the case of C_{12} the transition of the ground state between different spin sectors as a function of applied field can be tracked in the complex λ plane. However the trajectory of the zeros of $B_N^{a.c.}(\lambda)$, the off diagonal element in the effective Hamiltonian in equation (10), is different from C_{12} where the zeros move from the complex plane onto the real axis at $\lambda = 1$ and $h = h_c$ and then move away for $h > h_c$ as seen in figure 17. These values of λ are branch points of the energy function for the ground and first excited states. In C_{20} on the other hand close to the critical field, $h_c = 0.514$, two zeros of B approach the real λ axis from above and below at $\lambda \approx 0.85$. The critical field is the value of h where the triplet state first becomes the ground state at $\lambda = 1$. As h is increased further the two zeros move along the real axis in opposite directions, as shown in figure 26. At these values of λ there are discontinuous jumps in the value of $\langle S^z \rangle$ in the ground state as opposed to the rapid variation with λ as seen in C_{12} . These jumps occur as the ground and excited states with different values of $\langle S^z \rangle$ switch roles when $B_N^{a.c.}(\lambda)$ changes sign.

In figure 27 we plot $\langle S^z \rangle$ for the ground state as a function of applied magnetic field for different values of λ . The curves for $\lambda < 1$ are strongly reminiscent of the results for the magnetization of the classical approximations for C_{20} and C_{60} [13]. For $h > 0.5$ there are discontinuities in $\langle S^z \rangle$ for different values of λ . In these calculations starting from the field independent classical ground state the magnetic field is part of the perturbation and is scaled by λ . So the effective field at which discontinuities in $\langle S^z \rangle$ take place is λh . In the classical approximation for C_{20} there is a jump in the magnetization as a function of h at 1.43 equal to $0.68S_c$, where S_c is the magnitude of the classical spin. In the ground state calculated here the jump in $\langle S^z \rangle$ occurs for $\lambda \geq 0.72$ and grows in magnitude until, at $\lambda = 1$, the jump discontinuity in $\langle S^z \rangle$ is 1 for $h_c = 0.514$.

Different magnetic properties for the $S = \frac{1}{2}$ solutions of C_{12} and C_{20} are thus seen to come from the different analytic behavior of the wavefunctions in the complex λ plane. Similarity of the quantum solutions with the classical solutions suggests that this difference in analytic structure comes from the different connectivities of the two systems.

V. CONCLUSION

We have applied perturbation theory in the strength of quantum fluctuations around the classical ground states and found essentially exact results for the ground and first excited states for two frustrated spin systems, C_{12} and C_{20} . For C_{20} large orders in perturbation expansion and a high degree of numerical precision are required to get

convergence of the analytic continuation of the matrix elements of the effective Hamiltonian and the wavefunction coefficients calculated perturbatively.

We found that although sites in both systems are three-fold coordinated the spectra are qualitatively different with the lowest lying excited state being a triplet in C_{12} while it is a singlet in C_{20} . The difference in the behavior of the two systems is attributed to their difference in the connectivity. The average energies per nearest neighbor bond for $S = \frac{1}{2}$ spins, $-0.325J$ (in C_{20}) and $-0.3105J$ (in C_{12}), taking $J_1 = J_2 = J$, are comparable so that the “average” degree of frustration is the same for both systems. In C_{12} the first excited state arises by taking a linear combination of states each associated with a triplet excitation of a single non-triangle bond. By comparing $\langle \vec{S}_1 \cdot \vec{S}_4 \rangle$ in figures 14 and 15 the non-triangle bond is seen to take on a more strongly triplet character in the excited state. In C_{20} on the other hand there is no nearest neighbor bond which can be singled out to describe the character of the singlet and triplet excited states. The different values of \vec{S}^2 for states in C_{20} arise from small changes in long range correlations. In order to distinguish between C_{12} and C_{20} we observe that in C_{20} all bonds are members of closed loops in which all bonds are equivalent while in C_{12} the non-triangle bonds form alternating sides with triangle bonds to make hexagons. However characterization of connectivity by the nature of bonds forming closed loops is not sufficient in itself since the excited state of the Heisenberg model on a cube has a triplet excited state.

In the classical approximation it was possible to characterize the ground state for different systems in terms of a topological number, the Skyrmion number, and to associate this with the presence or absence of discontinuities in the magnetization. We have shown that this difference, seen in the classical approximation for C_{12} and C_{20} , survives in S^z for the exact states of the isotropic $S = \frac{1}{2}$ Heisenberg model and that it is associated with the analytic behavior in the complex coupling constant plane. Although it seems clear that it is the combination of frustration and connectivity which is responsible for the nature of the spectrum and the response of the system to a magnetic field, how exactly these are determined is not obvious.

The connection between frustration and the character of the excitation spectrum is also of interest for infinite lattices. The apparent singlet nature of the excitation spectrum in the Kagomé lattice arises from frustration [18,26] and leads to a large non magnetic contribution to the entropy of the system at low temperatures. This is an important feature in analysis of experimental data on any physical realization of a Kagomé lattice. This result for the Kagomé lattice may not generalize to other frustrated lattices if the sensitivity to connectivity seen in C_{12} and C_{20} is a guide to larger systems [27].

The accuracy of the wavefunctions found at $\lambda = 1$ suggest that the Padé approximants derived from the perturbation series are very accurate representations of the wavefunctions and energies in the complex plane between the origin and $\lambda = 1$ and that the analytic structure of these functions accurately represents the dependence on λ and applied field. We have shown how the rapid change of $\langle S^z \rangle$ for $\lambda \simeq 1$ and $h \simeq h_c$ and the discontinuity in $\langle S^z \rangle$ for C_{20} can be traced back to the Padé approximants. The ability to track this order-disorder transition from coherent states to eigenstates of S^z and \vec{S}^2 as a function of λ and applied field may be developed for richer many body systems with the calculational resources available today.

These calculations are being extended to higher values of spin and to finite temperatures and will be used to investigate the temperature evolution of the properties of magnetic molecules, Mn_{12} , Fe_8 etc., and, in particular, the quantum mechanical description of the large moments presently used in their analysis [28].

D. Coffey thanks G. Baker, R. Singh and S. Trugman for discussions on some of the points raised in the calculations and D. C. Mattis for comments and suggestions on the manuscript. The authors thank N. Bock and M. Jones for technical assistance. Numerical calculations were performed on the machines of the Center of Computational Research at SUNY Buffalo.

- [1] E. Manousakis, Rev. Mod. Phys. **63**, 1 (1991).
- [2] S. Sachdev and M. Vojta, Physica B **280**, 333 (2000).
- [3] H.A. Bethe, Z.Phys. **71**, 205 (1931).
- [4] W. J. Caspers, *Spin Systems*, World Scientific (1989).
- [5] B. Bernu, P. Lecheminant, C. Lhuillier and L. Pierre, Phys. Rev. B **50**, 10048 (1994).
- [6] C. Lhuillier, P. Sindzingre and J.-B. Fouet, cond-mat/0009336.
- [7] D. C. Johnston, M. Troyer, S. Miyahara, D. Lidsky, K. Ueda, M. Azuma, Z. Hiroi, M. Takano, M. Isobe, Y. Ueda, M.A. Korotin, V.I. Anisimov, A.V. Mahajan and L.L. Miller, cond-mat/0001147 (2000).
- [8] M. P. Gelfand, R. R. P. Singh and D. A. Huse, Journal of Statistical Physics **59**, 1093 (1990).
- [9] D. C. Mattis, *The Theory of Magnetism I : Statics and Dynamics*, Springer (1988).

- [10] Q. F. Zhong and S. Sorella, *Europhys. Lett.* **21**, 629 (1993).
- [11] A. E. Trumper, L. Capriotti and S. Sorella, *Phys. Rev. B* **61**, 11529 (2000).
- [12] S. R. White, *Phys. Rev. Lett.* **69**, 2863 (1992).
- [13] D. Coffey and S.A. Trugman, *Phys. Rev. Lett.* **69**, 176 (1992).
- [14] N. A. Modine and E. Kaxiras, *Phys. Rev. B* **53**, 2546 (1996).
- [15] T. D. Lee and C. N. Yang, *Phys. Rev.* **87**, 410 (1952).
- [16] V. Matveev and R. Shrock, *Phys. Rev. E* **53**, 254 (1996).
- [17] M.P. Gelfand, *Solid State Commun.* **98**, 11 (1996).
- [18] M. Mambrini and F. Mila, *Eur. Phys. J. B* **17**, 651 (2000).
- [19] J. R. Klauder and B. Skagerstam, *Coherent States*, World Scientific (1985).
- [20] G.A. Baker, *Essentials Of Padé Approximants*, Academic Press (1975).
- [21] A. Cuyt and L. Wuytack, *Nonlinear Methods In Numerical Analysis*, North Holland (1987).
- [22] D. Coffey and S.A. Trugman, *Phys. Rev. B* **46**, 12717 (1992).
- [23] E. F. Shender and P. C. W. Holdsworth, in *Fluctuations and Order : The New Synthesis*, edited by M. Millonas, Springer Verlag (1996).
- [24] K.S.D. Beach, R.J. Gooding and F. Marsiglio, *Phys. Rev. B* **61**, 5147 (2000).
- [25] S. Chatterjee, <http://www.cs.unc.edu/Research/HARPOON/mpfun++/> , original Fortran version: D. H. Bailey, <http://www.nersc.gov/~dhh/mpdist/mpdist.html>
- [26] C. Waldtmann, H.-U. Everts, B. Bernu, C. Lhuillier, P. Sindzingre, P. Lecheminant, L. Pierre, *Eur. Phys. J. C* **2**, 501 (1998).
- [27] R. R. P. Singh, W. E. Pickett, D. W. Hone and D. J. Scalapino, *Comm. on Mod. Phys.* **2**, B1 (2000).
- [28] H. A. De Raedt, A. H. Harns, V. V. Dobrovitski, M. Al-Saqr, M. I. Katsnelson, B. N. Harmon, cond-mat/0006504.

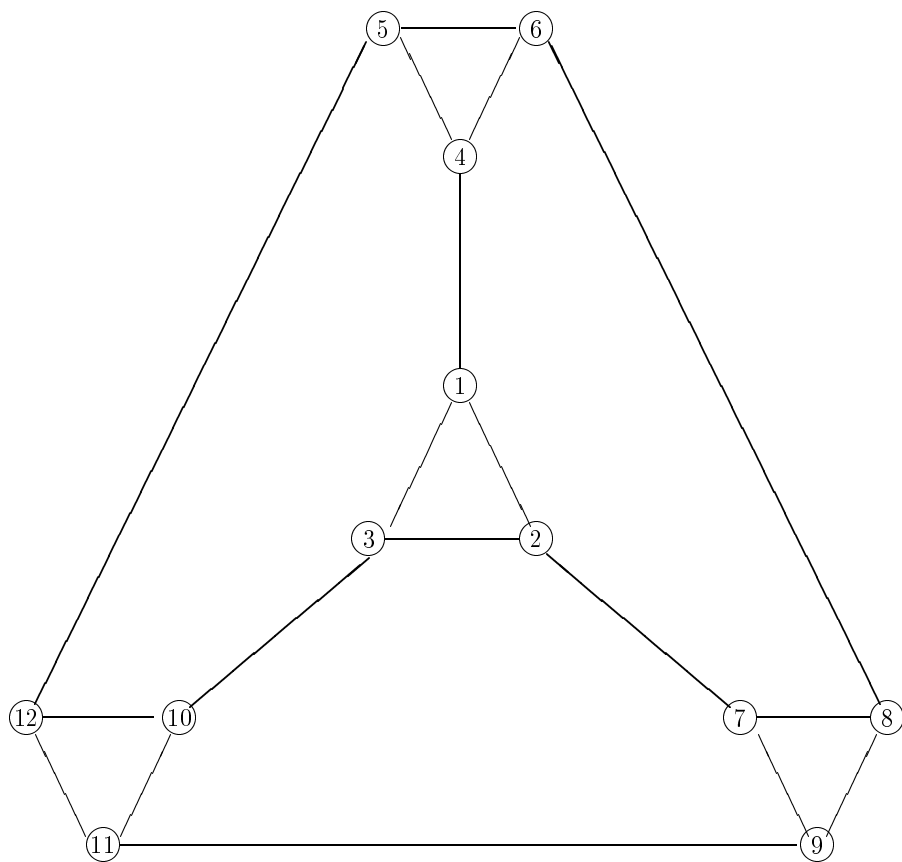


FIG. 1. Space configuration of C_{12} . Intra-triangle bonds are called J_1 , while inter-triangle bonds are called J_2 .

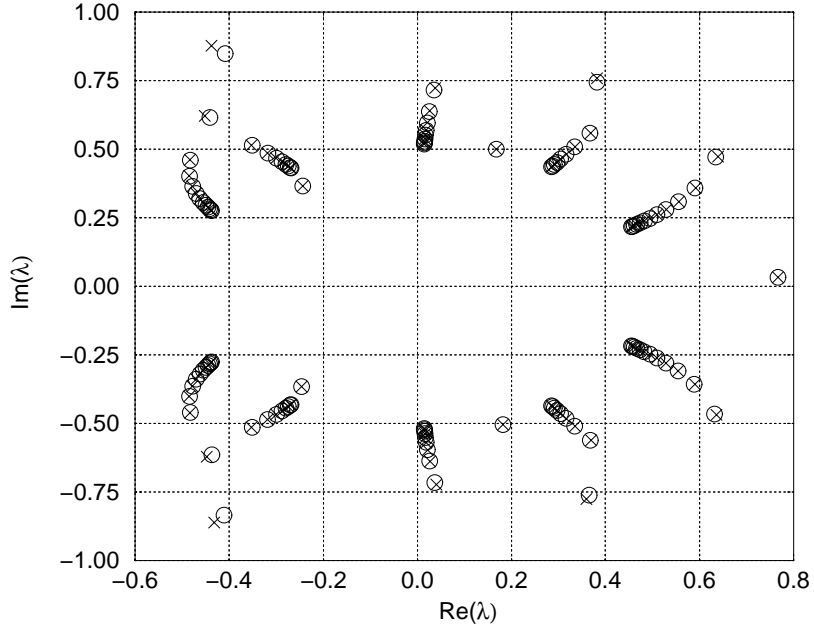


FIG. 2. Zeros and poles of the Padé approximant of the diagonal element A_N of the effective Hamiltonian for $\alpha = 1$ in C_{12} with 220 orders of perturbation theory used, \circ : zeros , \times : poles.

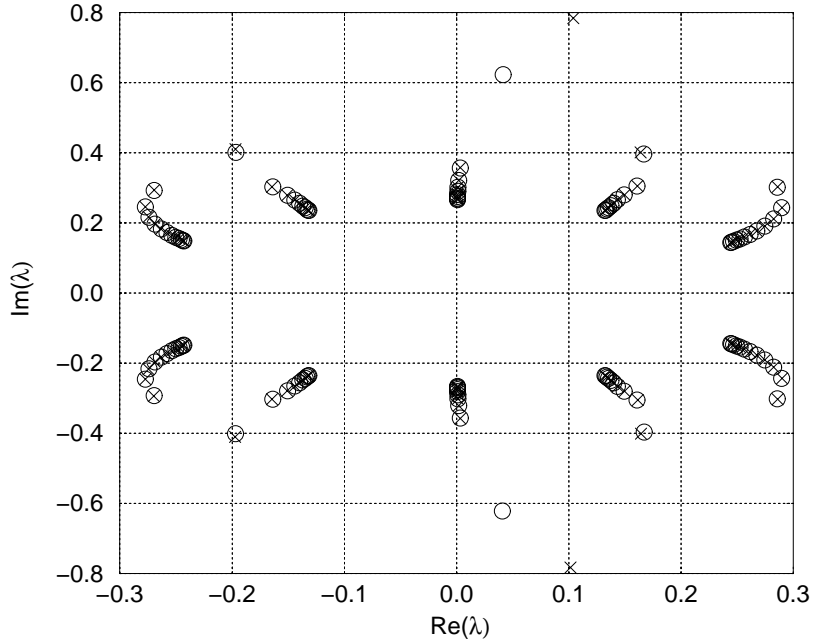


FIG. 3. Zeros and poles of the Padé approximant of the diagonal element A_N of the effective Hamiltonian for $\alpha = 2$ in C_{12} with 220 orders of perturbation theory used, \circ : zeros , \times : poles.

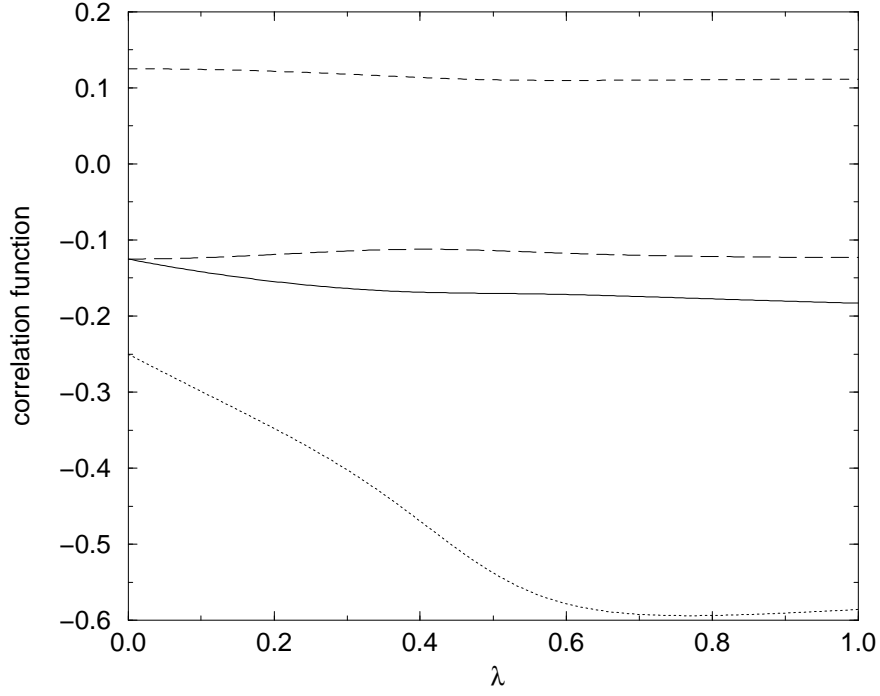


FIG. 4. Correlation functions for $J_2 = 1$ in the ground state of C_{12} at $h = 0$: solid line : $\langle \vec{S}_1 \cdot \vec{S}_2 \rangle$, dotted line : $\langle \vec{S}_1 \cdot \vec{S}_4 \rangle$, dashed line : $\langle \vec{S}_1 \cdot \vec{S}_5 \rangle$, long dashed line : $\langle \vec{S}_1 \cdot \vec{S}_8 \rangle$

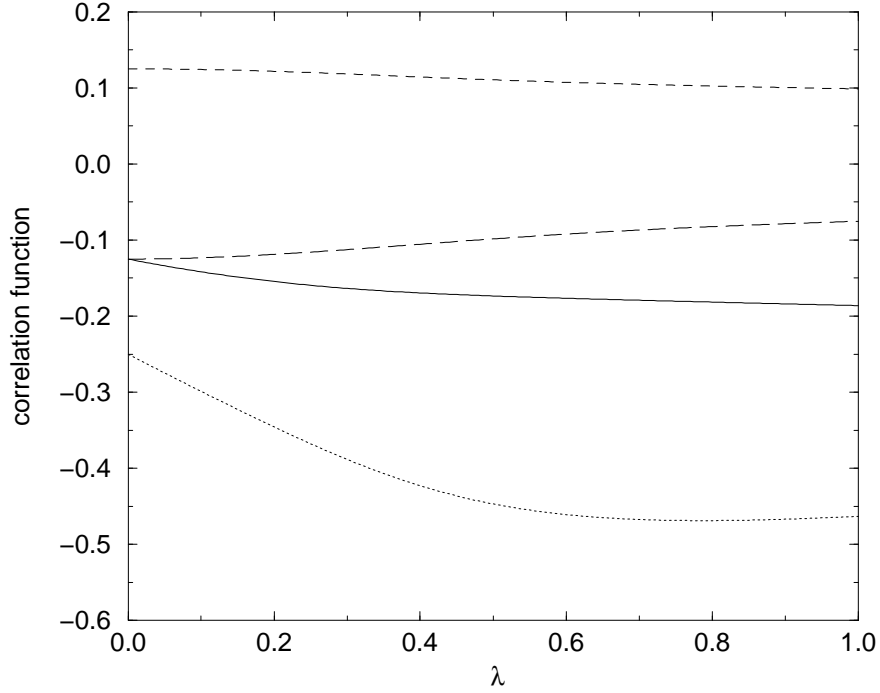


FIG. 5. Correlation functions for $J_2 = 1$ in the first excited state of C_{12} at $h = 0$: solid line : $\langle \vec{S}_1 \cdot \vec{S}_2 \rangle$, dotted line : $\langle \vec{S}_1 \cdot \vec{S}_4 \rangle$, dashed line : $\langle \vec{S}_1 \cdot \vec{S}_5 \rangle$, long dashed line : $\langle \vec{S}_1 \cdot \vec{S}_8 \rangle$

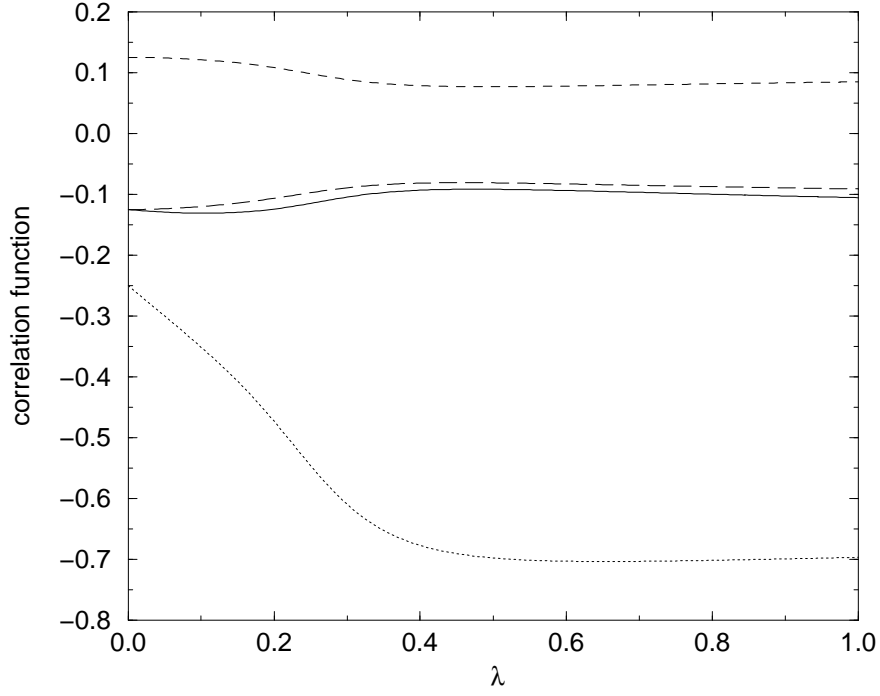


FIG. 6. Nearest neighbor correlation functions for $J_2 = 2$ in the ground state of C_{12} at $h = 0$: solid line : $\langle \vec{S}_1 \cdot \vec{S}_2 \rangle$, dotted line : $\langle \vec{S}_1 \cdot \vec{S}_4 \rangle$, dashed line : $\langle \vec{S}_1 \cdot \vec{S}_5 \rangle$, long dashed line : $\langle \vec{S}_1 \cdot \vec{S}_8 \rangle$

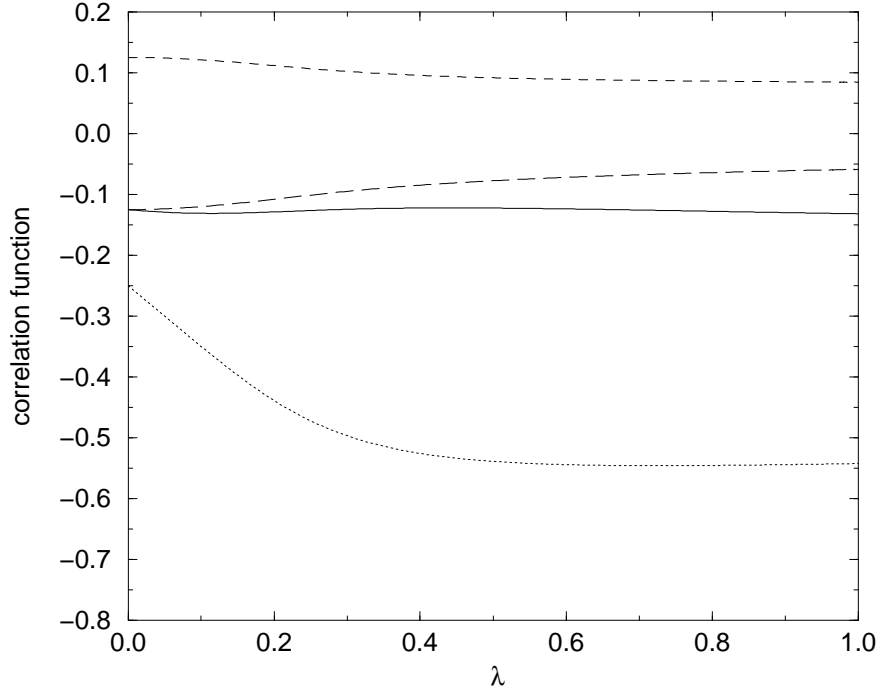


FIG. 7. Nearest neighbor correlation functions for $J_2 = 2$ in the $S = 1$, $S^z = 0$ first excited state of C_{12} at $h = 0$: solid line : $\langle \vec{S}_1 \cdot \vec{S}_2 \rangle$, dotted line : $\langle \vec{S}_1 \cdot \vec{S}_4 \rangle$, dashed line : $\langle \vec{S}_1 \cdot \vec{S}_5 \rangle$, long dashed line : $\langle \vec{S}_1 \cdot \vec{S}_8 \rangle$

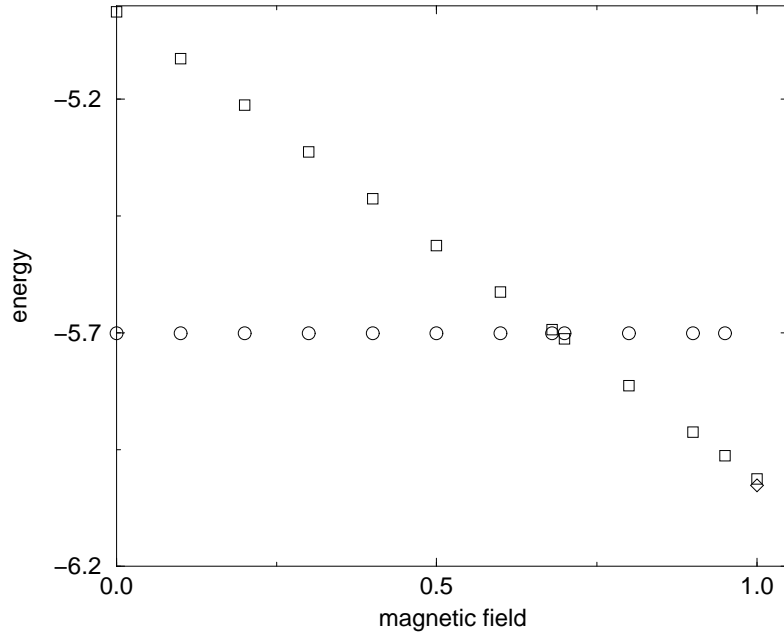


FIG. 8. Ground state and first excited state energy as a function of applied magnetic field for C_{12} , \circ : $S^z = 0$, \square : $S^z = 1$, \diamond : $S^z = 2$.

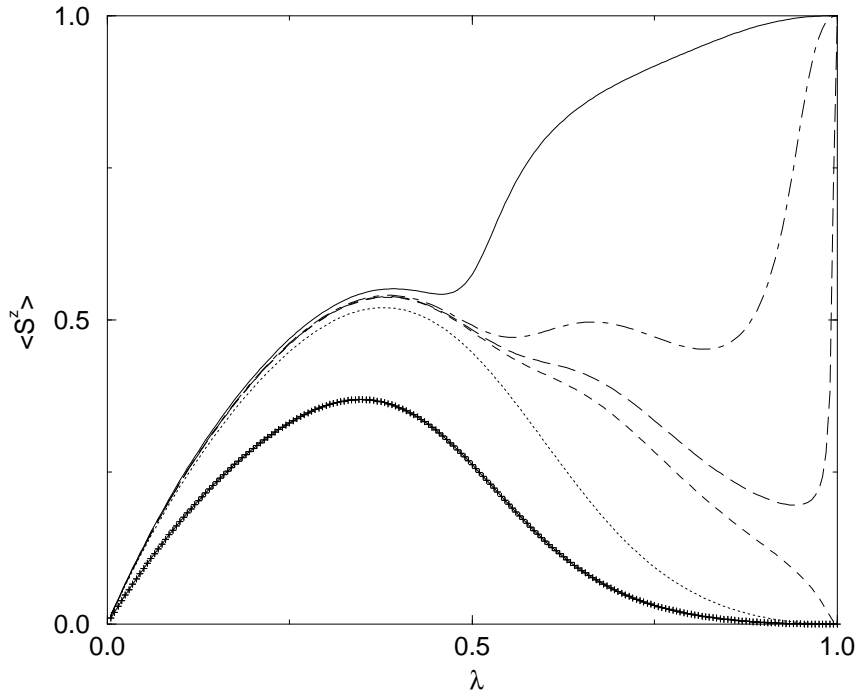


FIG. 9. S^z vs. λ for C_{12} for a magnetic field h (ground state) starting from the magnetic field independent classical ground state , $J_2 = 1.0$, solid-plus line : $h=0.500$, dotted line : $h=0.670$, dashed line : $h=0.687$, long dashed line : $h=0.688$, dot-dashed line : $h=0.690$, solid line : $h=0.700$.

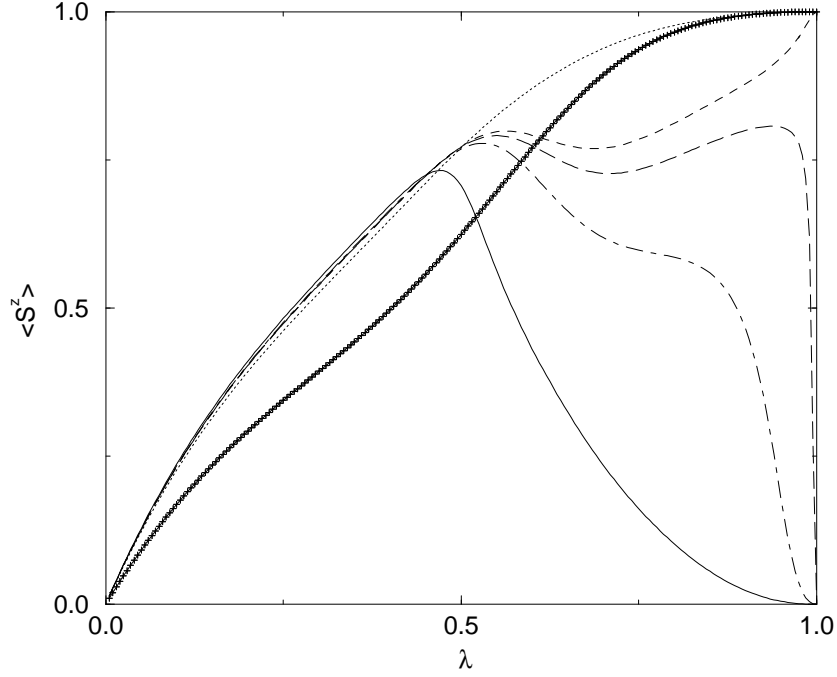


FIG. 10. S^z vs. λ for C_{12} for a magnetic field h (excited state) starting from the magnetic field independent classical ground state , $J_2 = 1.0$, solid-plus line : $h=0.500$, dotted line : $h=0.670$, dashed line : $h=0.687$, long dashed line : $h=0.688$, dot-dashed line : $h=0.690$, solid line : $h=0.700$.

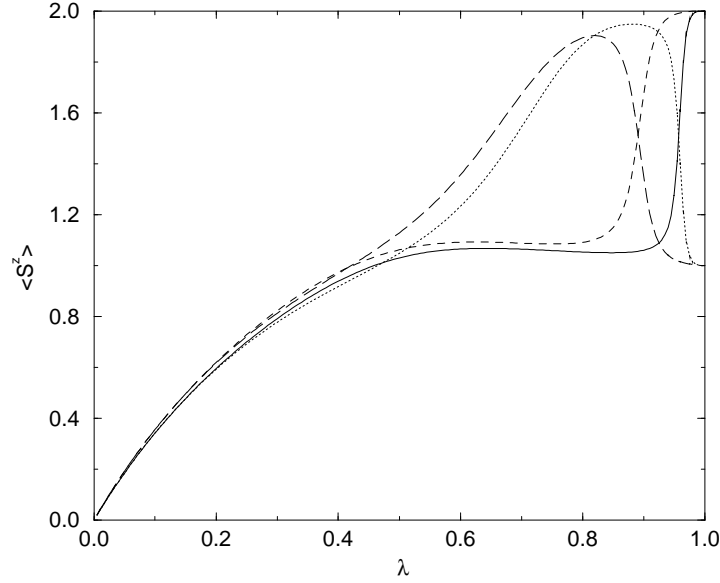


FIG. 11. S^z vs. λ for C_{12} for a magnetic field h starting from the magnetic field independent classical ground state , $J_2 = 1.0$, solid line : $h=1.010$, ground state , dotted line : $h=1.010$, excited state , dashed line : $h=1.050$, ground state , long dashed line : $h=1.050$, excited state.

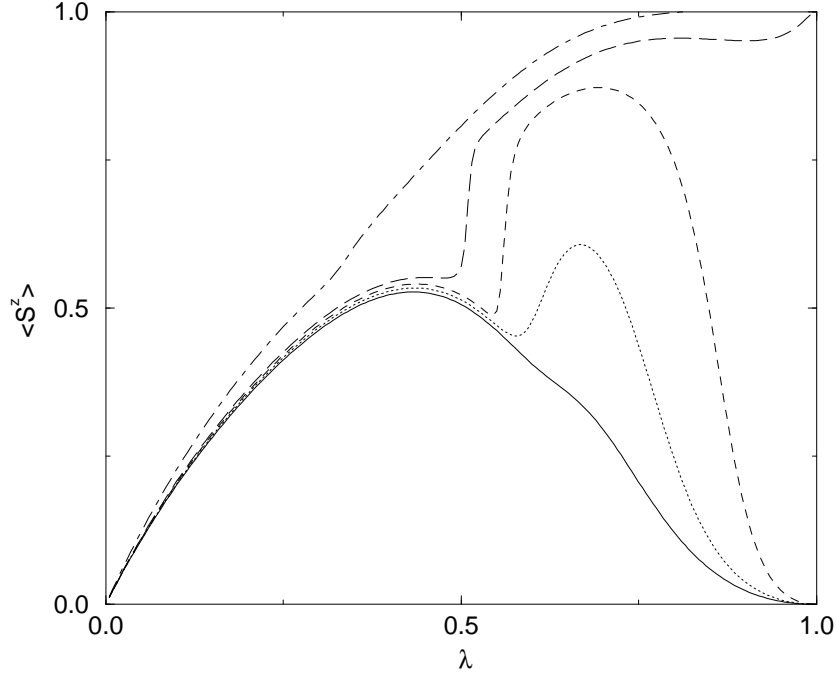


FIG. 12. S^z vs. λ for C_{12} for a magnetic field h starting from the magnetic field independent classical ground state, $J_2 = 0.8$, solid line : $h=0.530$, dotted line : $h=0.535$, dashed line : $h=0.540$, long dashed line : $h=0.547$, dot-dashed line : $h=0.600$.

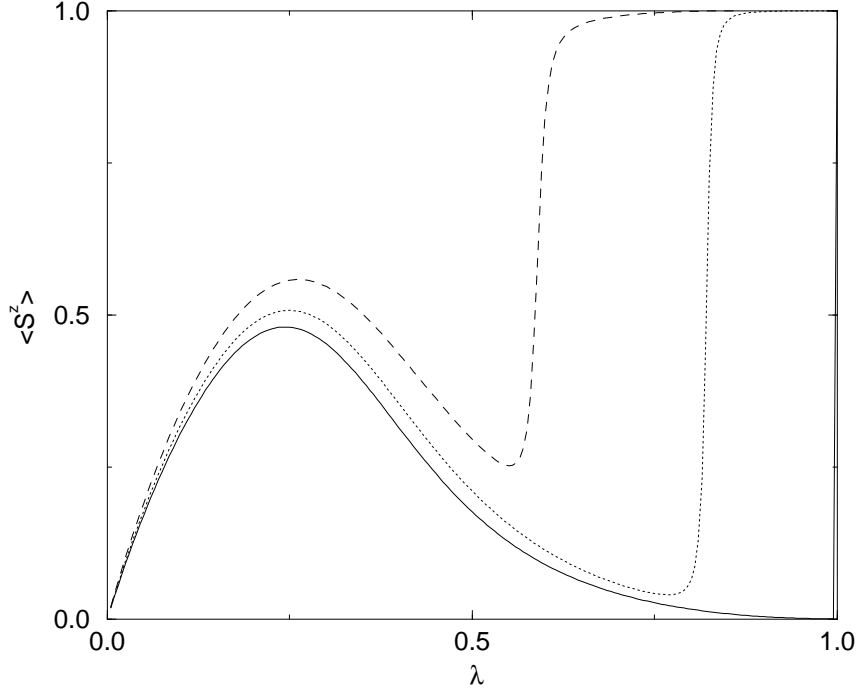


FIG. 13. S^z vs. λ for C_{12} for a magnetic field h starting from the magnetic field independent classical ground state, $J_2 = 1.8$, solid line : $h=1.3423$, dotted line : $h=1.400$, dashed line : $h=1.500$.

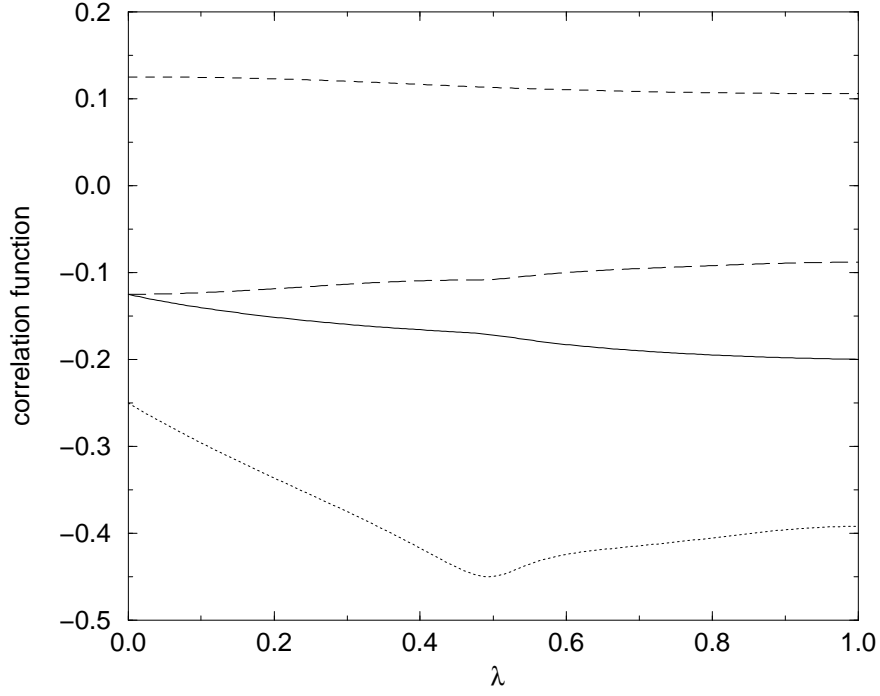


FIG. 14. Nearest neighbor correlation functions for C_{12} for $J_2 = 1$, $h = 0.7$, ground state : solid line : $\langle \vec{S}_1 \cdot \vec{S}_2 \rangle$, dotted line : $\langle \vec{S}_1 \cdot \vec{S}_4 \rangle$, dashed line : $\langle \vec{S}_1 \cdot \vec{S}_5 \rangle$, long dashed line : $\langle \vec{S}_1 \cdot \vec{S}_8 \rangle$

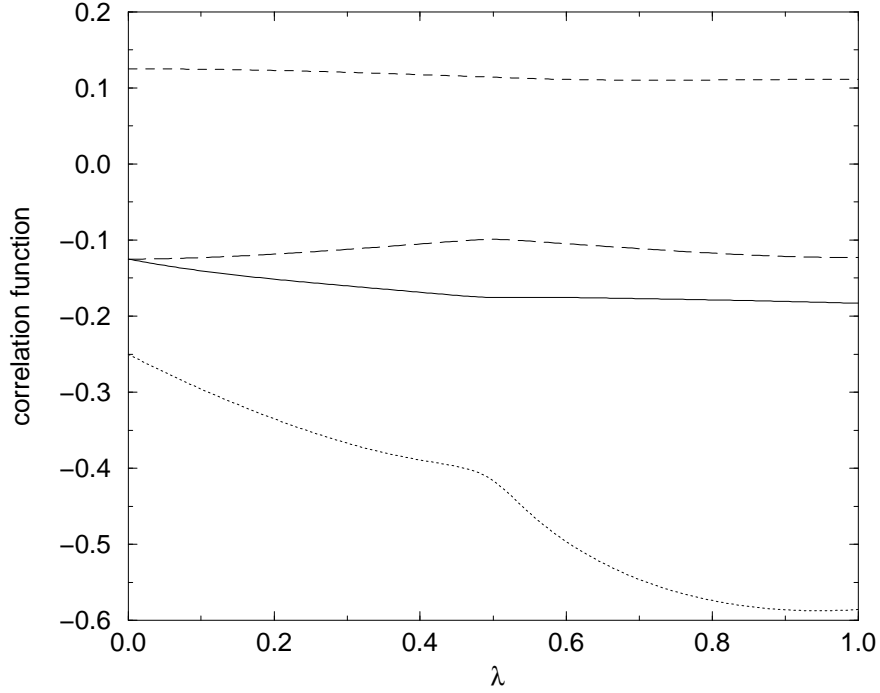


FIG. 15. Nearest neighbor correlation functions for C_{12} for $J_2 = 1$, $h = 0.7$, excited state : solid line : $\langle \vec{S}_1 \cdot \vec{S}_2 \rangle$, dotted line : $\langle \vec{S}_1 \cdot \vec{S}_4 \rangle$, dashed line : $\langle \vec{S}_1 \cdot \vec{S}_5 \rangle$, long dashed line : $\langle \vec{S}_1 \cdot \vec{S}_8 \rangle$

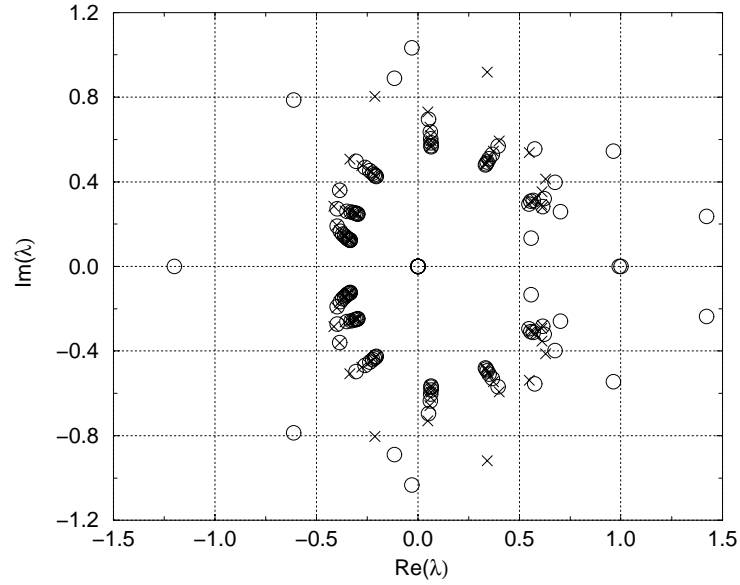


FIG. 16. Zeros and poles of the Padé approximant of the square root in C_{12} with 220 orders of perturbation theory used, magnetic field $h=0.688$, \circ : zeros , \times : poles.

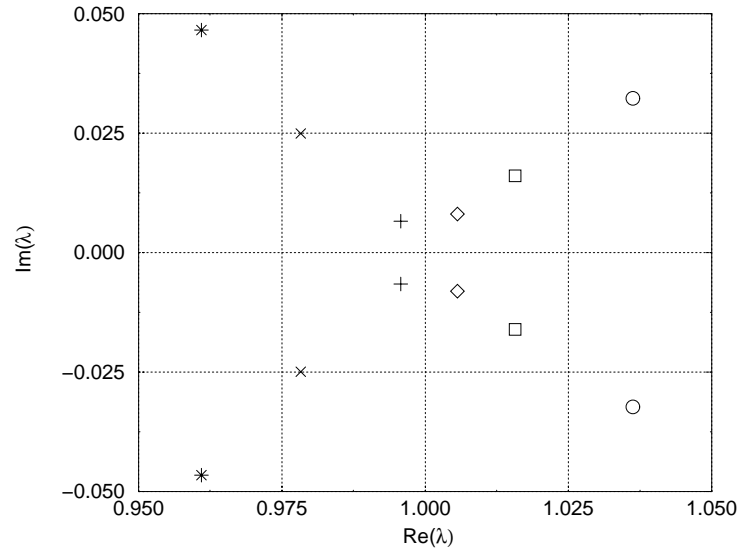


FIG. 17. Zeros of the Padé approximant for the square root using 270 orders of perturbation theory for various magnetic fields , \circ : $h=0.686$, \square : $h=0.687$, \diamond : $h=0.6875$, $+$: $h=0.688$, \times : $h=0.689$, $*$: $h=0.690$.

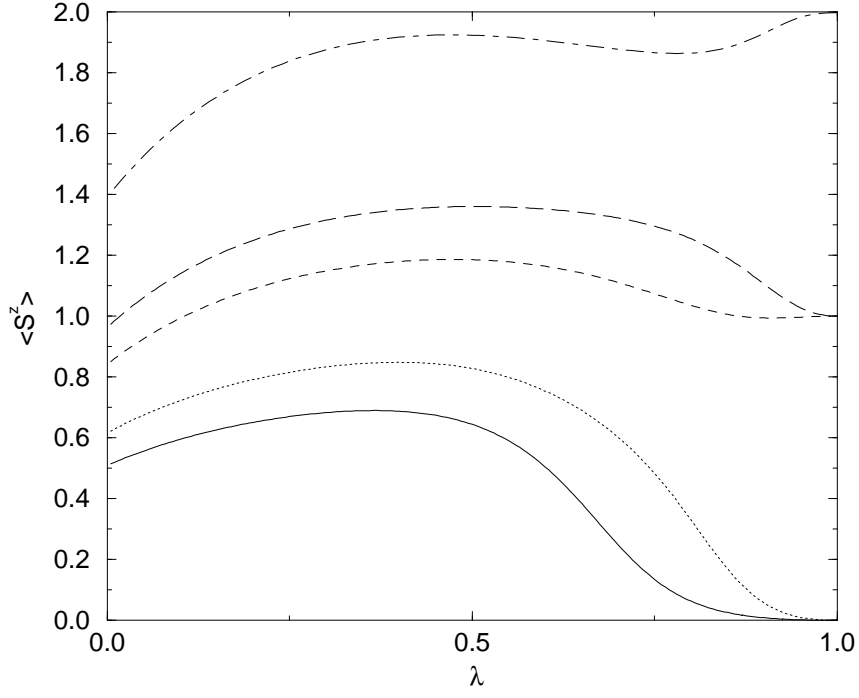


FIG. 18. S^z vs. λ for C_{12} for a magnetic field h starting from the magnetic field dependent classical ground state, $J_2 = 1.0$, solid line : $h=0.5$, dotted line : $h=0.6$, dashed line : $h=0.8$, long dashed line : $h=0.9$, dot-dashed line : $h=1.200$.

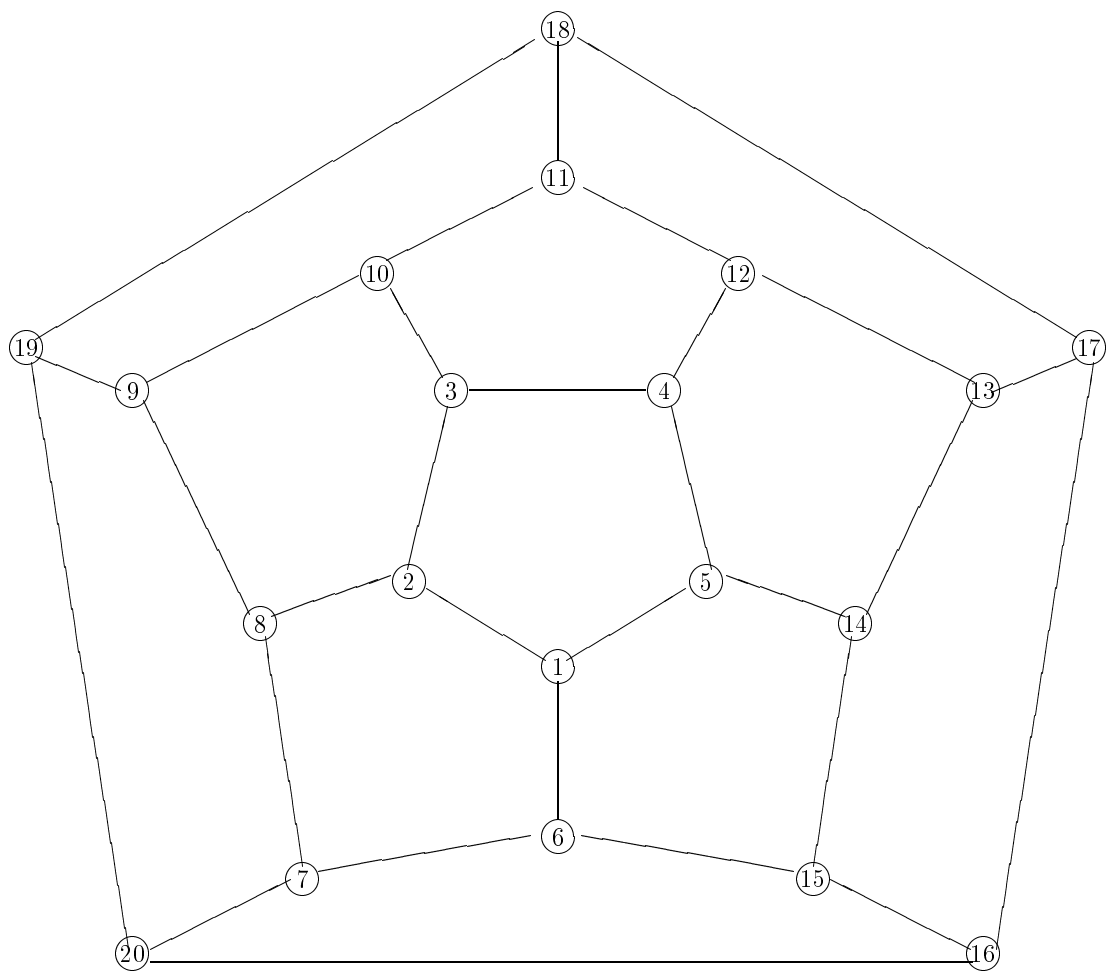


FIG. 19. Space configuration of C_{20} . All the bonds are equal to J .

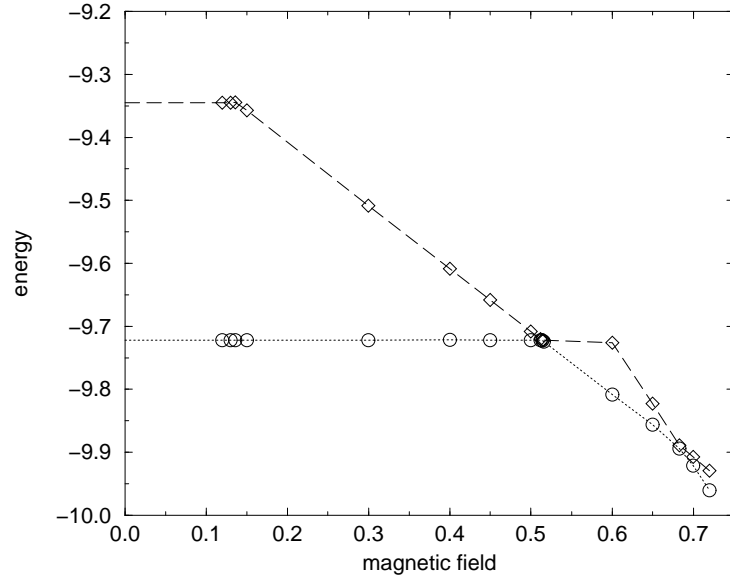


FIG. 20. Ground state and first excited state energy for different values of applied magnetic field for C_{20} , \circ : ground state, \diamond : excited state. The dotted line is a fit for the ground state, and the long dashed line for the excited state.

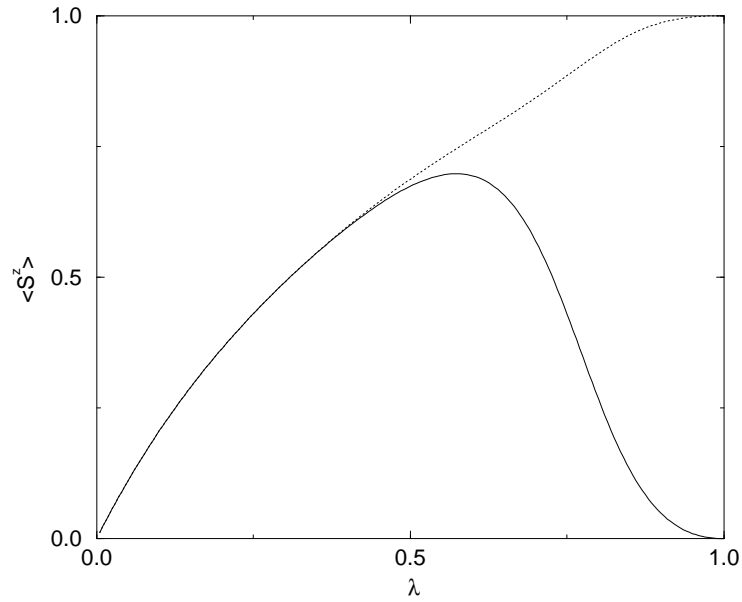


FIG. 21. $\langle S^z \rangle$ as a function of λ for the ground state and first excited state of C_{20} for a magnetic field $h = 0.4$ starting from the magnetic field independent classical ground state, solid line : ground state, dotted line : excited state.

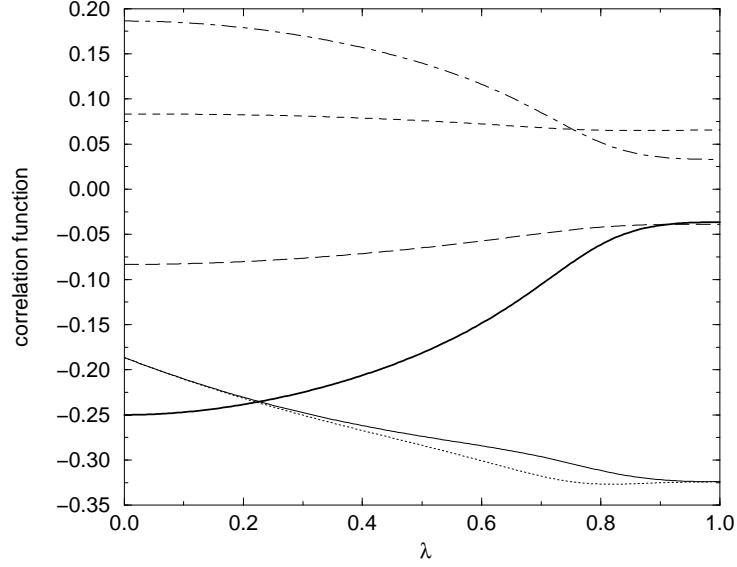


FIG. 22. Spin correlations in the ground state of C_{20} as a function of λ for $h=0.4$: solid line : $\langle \vec{S}_1 \cdot \vec{S}_2 \rangle$, dotted line : $\langle \vec{S}_1 \cdot \vec{S}_6 \rangle$, dashed line : $\langle \vec{S}_1 \cdot \vec{S}_3 \rangle$, long dashed line : $\langle \vec{S}_1 \cdot \vec{S}_9 \rangle$, dot-dashed line: $\langle \vec{S}_1 \cdot \vec{S}_{11} \rangle$, thick solid line: $\langle \vec{S}_1 \cdot \vec{S}_{18} \rangle$.

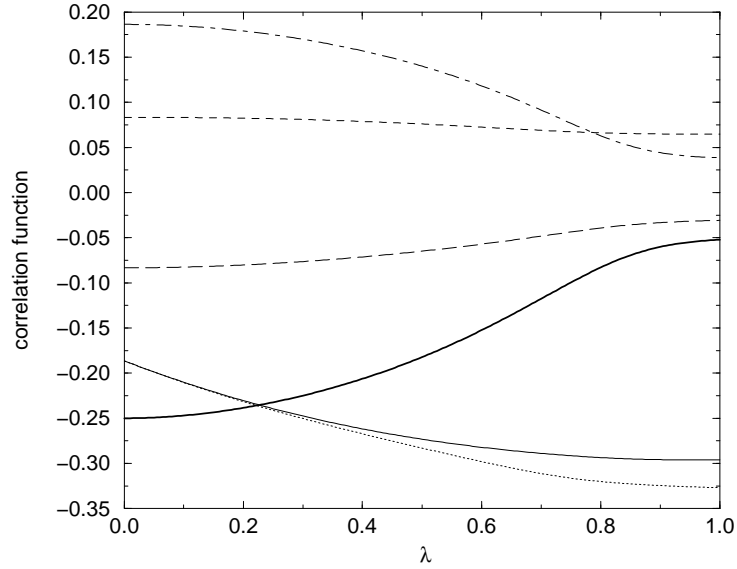


FIG. 23. Spin correlations in the first excited state of C_{20} as a function of λ for $h=0.4$: solid line : $\langle \vec{S}_1 \cdot \vec{S}_2 \rangle$, dotted line : $\langle \vec{S}_1 \cdot \vec{S}_6 \rangle$, dashed line : $\langle \vec{S}_1 \cdot \vec{S}_3 \rangle$, long dashed line : $\langle \vec{S}_1 \cdot \vec{S}_9 \rangle$, dot-dashed line: $\langle \vec{S}_1 \cdot \vec{S}_{11} \rangle$, thick solid line: $\langle \vec{S}_1 \cdot \vec{S}_{18} \rangle$.

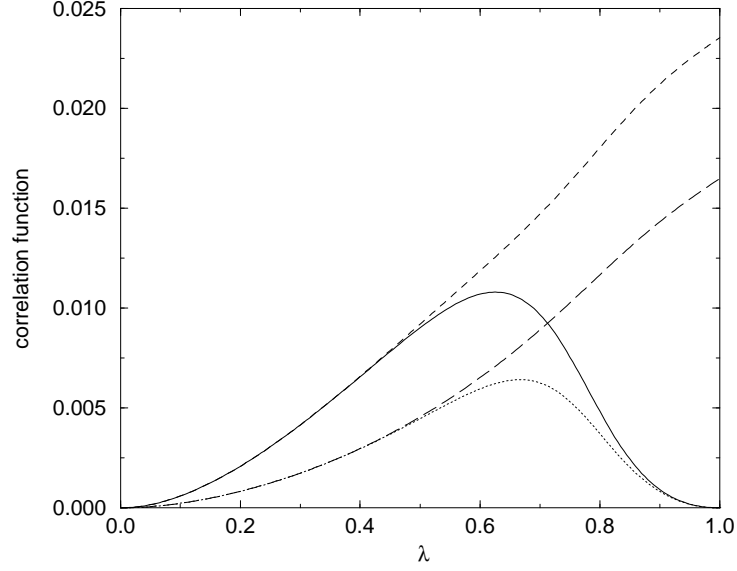


FIG. 24. Ground and excited state spin correlations for $h = 0.4$ as a function of λ for C_{20} at sites $i=1$ and $i=6$: solid line : $\langle \vec{S}_1 \cdot \vec{h} \rangle$ in the ground state, dotted line : $\langle \vec{S}_6 \cdot \vec{h} \rangle$ in the ground state, dashed line : $\langle \vec{S}_1 \cdot \vec{h} \rangle$ in the excited state, long dashed line : $\langle \vec{S}_6 \cdot \vec{h} \rangle$ in the excited state.

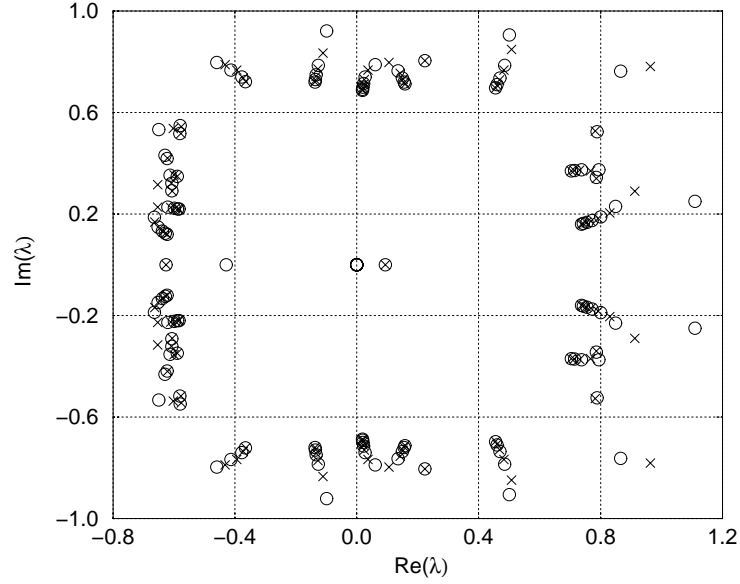


FIG. 25. Zeros (o) and poles (x) of the Padé approximant $B_N^{a,c}(\lambda)$ in the complex λ plane for C_{20} in an applied field $h = 0.3$, 240 orders of perturbation theory were used.

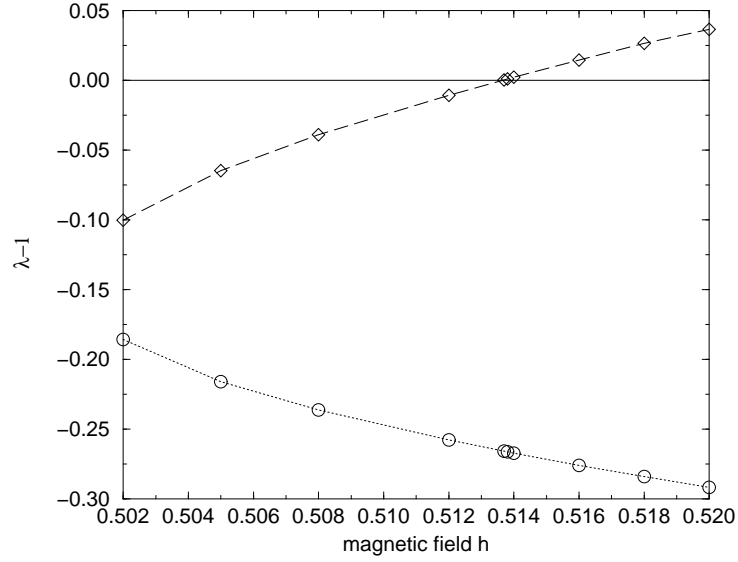


FIG. 26. Zeros of the Padé approximant $B_N^{a,c}(\lambda)$ along the λ real axis for C_{20} . 240 orders of perturbation theory were used and \circ and \diamond are the values calculated. The dotted and long-dashed lines are fits.

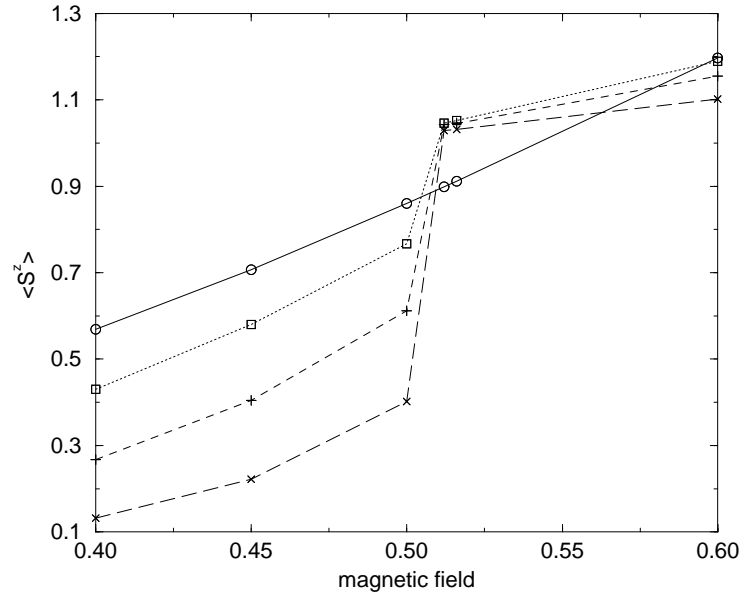


FIG. 27. $\langle S^z \rangle$ as a function of magnetic field for the ground state of C_{20} for various λ 's : \circ : $\lambda = 0.70$, \square : $\lambda = 0.75$, \triangle : $\lambda = 0.80$, \times : $\lambda = 0.85$. The lines are fits.